Communications in Theoretical Physics

Commun. Theor. Phys. **76** (2024) 125401 (20pp) https://doi.org/10.1088/1572-9494/ad641d

Casimir wormholes inspired by electric charge in Einstein–Gauss–Bonnet gravity

Mushayydha Farooq[1], **M Zubair**[1,2,*], **Ali H Alkhaldi**[3] **and Akram Ali**[3]

[1] Department of Mathematics, COMSATS University Islamabad, Lahore Campus, Lahore, Pakistan
[2] National Astronomical Observatories, Chinese Academy of Sciences, Beijing 100101, China
[3] Department of Mathematics, King Khalid University, 9004 Abha, Saudi Arabia

E-mail: Mushayydha_90@hotmail.com, mzubairkk@gmail.com, drmzubair@cuilahore.edu.pk, ahalkhaldi@kku.edu.sa and akali@kku.edu.sa

Received 14 March 2024, revised 2 July 2024
Accepted for publication 12 July 2024
Published 14 October 2024

Abstract

This investigation assesses the feasibility of a traversable wormhole by examining the energy densities associated with charged Casimir phenomena. We focus on the influence of the electromagnetic field created by an electric charge as well as the negative energy density arising from the Casimir source. We have developed different shape functions by defining energy densities from this combination. This paper explores various configurations of Casimir energy densities, specifically those occurring between parallel plates, cylinders and spheres positioned at specified distances from each other. Furthermore, the impact of the generalized uncertainty principle correction is also examined. The behavior of wormhole conditions is evaluated based on the Gauss–Bonnet coupled parameter (μ) and electric charge (Q) through the electromagnetic energy density constraint. This is attributed to the fact that the electromagnetic field satisfies the characteristic $\rho = -p_r$. Subsequently, we examine the active gravitational mass of the generated wormhole geometries and explore the behavior of μ and Q concerning active mass. The embedding representations for all formulated shape functions are examined. Investigations of the complexity factor of the charged Casimir wormhole have demonstrated that the values of the complexity factor consistently fall within a particular range in all scenarios. Finally, using the generalized Tolman–Oppenheimer–Volkoff equation, we examine the stability of the resulting charged Casimir wormhole solutions.

Keywords: charged casimir wormholes, GUP-Corrected casimir wormholes, modified gravity

(Some figures may appear in colour only in the online journal)

1. Introduction

Wormholes (WHs) or Einstein–Rosen bridges are topological objects that link various places within the same spacetime or even separate spacetimes, as predicted by general relativity (GR), a theory that explains gravity in terms of geometry. These objects resemble a tube with flat ends in an asymptotically flat shape, and they act as shortcuts between these regions. In 1935, a particular kind of WH solution was first proposed by Einstein and Rosen, known as the 'Einstein–Rosen bridge' [1]. The Einstein–Rosen WH was formerly thought to be non-traversable. Morris and Thorne [2] proposed a WH spacetime that could be traversed under the condition known as the 'flare-out condition.' Morris and Thorne were the first to discuss the topic of WH traversability. This solves the non-traversable WH issue, according to [3]. Morris and Thorne introduced the idea of exotic matter with a negative energy density within the framework of GR to maintain the traversability of WHs. Building on the groundbreaking work of Morris and Thorne, numerous studies on traversable WH solutions have been carried out in the last 20 years [4–9].

Although it is commonly known that GR adequately characterizes the cosmos, certain new studies call for changing it to a more satisfactory alternative theory of gravity so as to explain the late-time acceleration expansion [10–13].

* Author to whom any correspondence should be addressed.

Consequently, other modified theories (for instance, $f(R)$ gravity [14, 15], $f(R, T)$ gravity [16], etc.) have been developed to overcome these issues. WH geometry has been extensively investigated in the context of modified theories of gravity [17–23]. Several intriguing pieces of research on WHs resembling Kerr's WH and their shadows have been published [24–26]. Additionally, WHs within the background of modified gravity have been explored in the literature; examples include those involving higher-order curvature invariants and higher-dimensional cosmological WHs [27]. These studies illustrate that these WHs can satisfy the energy criteria, at least at the throat [28–32]. According to research in the setting of modified gravity, it is quite possible to force matter to obey all energy restrictions as it passes through the throat of a WH. These nonstandard WH geometries are supported by higher-order curvature components, which can be considered as gravitational fluid. The D-dimensional Lorentzian WH solutions [33] investigated within the framework of Lovelock gravity, the generalized theory of gravitation in D dimensions [34], are of great significance. The radius of the WH throat was discovered to have a lower limit determined by the Lovelock parameter, spacetime dimension and the shape function (SF), compared with Einstein gravity. Moreover, it was demonstrated that higher-order Lovelock expressions expand the area of normal matter close to the throat with negative coupling constant.

As a second-order formulation of Lovelock gravity, the Einstein–Gauss–Bonnet (EGB) theory of gravitation in D dimensions has also been studied, as well as its connections to Lorentzian WH solutions [35]. It was determined that the characteristics of these WHs depend on the spacetime's dimensionality D and the Gauss–Bonnet (GB) coupling parameter (μ). The WH throat radius was demonstrated to often be restricted by D and μ. It was also investigated whether it was possible to find WH solutions restricted to the neighborhood around the throat. Compared with the GR scenario, the weak energy condition (WEC) is violated only for $\mu > 0$. In the case of $\mu < 0$, violation of this inequality depends upon the SF, modulus value of μ, D and radius r. Moreover, compact extra dimensions for dynamic WH solutions in the Lovelock gravity framework have been studied [36]. Aside from that, it has been demonstrated that the WEC is true for a particular range of the theory's coupling parameter. We recommend the reader to study these sources [37, 38] for further details on other higher-dimensional WH dynamics. The exotic matter content of the traversable WH is what preserves its stability. There is no doubt that exotic WH matter violates the null energy condition (NEC). NEC breach has been avoided or minimized in several works in the literature. In [39], Morris–Thorne static traversable WH solutions are studied in different modified theories of gravity, including quadratic, power-law, log-corrected and exponential hybrid metric–Palatini gravity. It was found that the NEC is violated in all these theories, indicating that exotic matter is required to support the WH. The possibility of minimizing the amount of exotic matter required to support the WH has also been discussed by adjusting the parameters of the modified gravity theories. In [40, 41], it was shown that the presence of the GB invariant in EGB can reduce or eliminate the need for exotic matter with negative energy density, which is typically required to support WHs. Moreover, in four-dimensional EGB gravity, the relationship of the SF was established and the behavior of μ for all ranges studied in [42].

In a recent study, Herrera [43] explored an anisotropic self-gravitating system to ascertain the vanishing complexity factor (CF). The Tolman mass and structure scalars were examined using the orthogonal splitting of the Riemann tensor. Furthermore, in 2009 Herrera *et al* [44] investigated the significant consequences of gravitational collapse, focusing in particular on the Israel–Stewart idea for viscous dissipative analysis using bulk shear viscosity. Regarding the context of the post-quasistatic estimate, Herrera *et al* [45] investigated the solutions of self-relativistic gravitational collapse within dissipative scenarios. Additionally, Herrera and Santos [46] investigated gravitational collapse within the Misner and Sharp framework, expanding their findings to the dissipative situation with free radiation streaming and heat movement. Furthermore, Herrera *et al* [47] focused on the equations characterizing the actual state with diminishing spatial gradients of energy densities in the conclusion of their study, which examined self-gravitating collapsing sources with anisotropic matter distribution. In 2019, the CF for a system in EGB gravity was computed by Sharif *et al* [48]. Moreover, Abbas and Ahmed [49] explored the the system to analyze its complexity for a certain class of compact structure within the background of $f(R, T)$ gravity. Further, Abbas and Nazar [50] concentrated on investigating the complex system for an anisotropic solution with a non-minimally coupled system in the framework of $f(R)$ gravity.

Notably, Garattini [51] proposed a static traversable WH model that explored the Casimir effect, including negative energy density, while taking into account the constraints imposed by the quantum WEC. In laboratory settings, Casimir energy is the only artificially produced source of exotic matter that is practical, and the geometry of barriers has a significant impact on its size. In particular, the vacuum's quantum field is warped in the presence of two uncharged flat parallel plates, resulting in a negative energy density that may act as a source for traversable WHs. The idea of a minimum length, recently discovered and thought to be of the order of the Planck length, is another notable feature of quantum physics. The precise measurement of tiny distances within spacetime is constrained by the existence of a minimum length scale. In quantum gravity theories, where the idea of minimal positional uncertainty is relevant, this inherent limitation automatically develops. The standard position–momentum uncertainty relation must be adjusted to account for the notion of a minimal length. The negative Casimir energy density is reinterpreted in light of the generalized uncertainty principle (GUP). It should be highlighted that the precise redefinition of the Casimir energy density will depend on the unique properties and configuration of maximally restricted quantum states. With this knowledge, it becomes exciting to incorporate the implications of the GUP into models of traversable WHs. Although the Casimir effect for parallel plates has been widely investigated, estimating the

Casimir force when the form of the conductors changes becomes much more difficult. While accurate outcomes are accessible for certain situations, such as the case of two concentric cylinders or spheres, other cases involve the employment of approximative techniques. Two frequently used approximation strategies in such circumstances are the proximity force approximation (PFA) and the multiple scattering approach.

Jusufi *et al* [52] have investigated how the GUP affects Casimir WHs, where the only source of exotic matter is the negative Casimir energy density. In another publication, the concept of Einstein–Rosen bridges or WHs has been explored by incorporating the notion of the GUP or minimal length [53]. Similarly, Javed *et al* [54] worked on the weak deflection angle of light coming out of Casimir WHs in the background of the weak field limit. Tripathy [55] also investigated Casimir WHs and GUP-corrected Casimir WHs in $f(R, T)$ modified gravity. Sokoliuk *et al* [56] worked on the possibility of a Casimir WH with zero tidal forces in the context of modified gravity theories. Muniz *et al* [57] studied the Casimir energy density in the spacetimes of rotating WHs. Other authors also investigated the Casimir WH scenario using three distinct Casimir energy densities, including parallel plates, parallel cylindrical plates and spheres [58]. Avalos *et al* [59] developed traversable WH geometries using the CF.

Garattini [60] examined the connection between Casimir energy and the capability of WHs. The relationship between an electromagnetic field produced by an electric charge and the induction of a negative energy density through the Casimir effect is the main subject of that article. Combining these two phenomena results in the introduction of an electro-vacuum source with a new parameter related to the WH throat. Motivated by this idea, in the present article we study the effects of an electric charge on Casimir WHs using four Casimir energy densities in EGB gravity. Additionally, we specifically explore the energy densities coming from the Casimir source, taking the GUP effects into account. The current paper is arranged as follows. First we discuss the fundamental outline of EGB gravity in section 2. The Casimir effect in the presence of an electric charge is the main topic of section 3. We develop SF from four different Casimir energy density scenarios in this section. We calculate the active mass for our WH solutions in section 4. Section 5 presents the embedding diagrams of the charged Casimir wormhole (CCWH). The behavior of the CF is covered in section 6, whereas section 7 shows the equilibrium forces of the discovered WH solution. Finally, we summarize our results in section 8.

2. Formulation and fundamental structure of field equations

The formulation of the action in the background of EGB gravity is expressed as follows:

$$\mathcal{I}_{\mathcal{G}} = \int \mathrm{d}^{D}x\sqrt{-g}\,(R + \mu_1\mathcal{G}). \tag{1}$$

Here, R defines the Ricci scalar, the dimension of spacetime is expressed by D and μ_1 acts as the GB coefficient. The expression for the GB invariant is represented by $\mathcal{G}$ and is expressed as follows:

$$\mathcal{G} = R^2 - 4R_{\alpha\beta}R^{\alpha\beta} + R_{\alpha\beta\delta\eta}R^{\alpha\beta\delta\eta}. \tag{2}$$

Now, by varying the action with respect to the metric tensor, one can deduce the field equations (FE) as follows:

$$G_{\alpha\beta} + \mu_1\mathcal{H}_{\alpha\beta} = \mathcal{T}_{\alpha\beta}, \tag{3}$$

In this context, $G_{\alpha\beta}$ denotes the Einstein tensor, $\mathcal{H}\alpha\beta$ defines the GB tensor and $\mathcal{T}\alpha\beta$ represents the energy–momentum tensor (EMT). The expression for $\mathcal{H}_{\alpha\beta}$ is articulated as follows:

$$\begin{aligned}\mathcal{H}_{\alpha\beta} = -\frac{1}{2}\times\mathcal{G}\times g_{\alpha\beta} + 2\times[R\times R_{\alpha\beta} - 2\\ \times R_{\alpha\sigma}\times R^{\sigma}_{\beta} - 2\times R_{\alpha\rho\beta\nu}\times R^{\rho\nu}\\ -2\times R_{\alpha abc}\times R^{abc}_{\beta}].\end{aligned} \tag{4}$$

We have assumed that $8\pi G_D = 1$, where G_D denotes the gravitational constant in D dimensions. For a $D-2$ sphere, WH geometry is written as

$$\mathrm{ds}^2 = \left(1 - \frac{b(r)}{r}\right)^{-1}\mathrm{dr}^2 + r^2\mathrm{d}\Omega^2_{D-2} - \mathrm{e}^{2\Phi(r)}\mathrm{dt}^2, \tag{5}$$

where $d\Omega^2_{D-2}$ displays WH spacetime for a $D-2$ sphere. The symbol $\Phi(r)$ shows the redshift function (RSF), signifying its association with gravitational redshift. Gravitational redshift is described as the frequency that a photon must possess to be recovered from a gravitational potential. It is essential to recognize that a photon does not possess sufficient energy to break free from an event horizon within a WH. To overcome this horizon, it is necessary for the RSF to remain finite across the entire domain. The shape of the WH is represented by the SF, denoted by the symbol $b(r)$. According to Morris and Thorne [2], the embedding diagram serves as a tool for visualizing the structure of the WH. The radial coordinate r depends on both the SF and RSF. The range of the radial coordinate is defined as $r_0 \leqslant r < \infty$, with r_0 representing the throat of the WH. Several conditions must be met to ensure the feasibility of traversable WH geometry. The specified conditions are articulated as follows:

- At the throat point, which is r_0, the condition for the WH is expressed as $b(r_0) = r_0$.
- The flaring out condition dictates that $b'(r_0) < 1$, where the prime indicates a derivative with respect to r.
- At higher values of r, i.e. $r \to \infty$, the constraint for achieving asymptotic flatness (AF) is defined as $\frac{b(r)}{r} \to 0$. As $r \to \infty$, this condition can be restated as $1 - \frac{b(r)}{r} > 0$.

We have used equation (5) and equation (3) to represent the FE of EGB gravity in the following manner:

$$\rho(r)=\frac{(D-2)}{2r^2}\left[\left(1+\frac{2\mu b(r)}{r^3}\right)\left(b'(r)-\frac{b(r)}{r}\right)+\frac{b(r)}{r}\left((D-3)+(D-5)\frac{\mu b(r)}{r^3}\right)\right], \tag{6}$$

$$p_r(r)=\frac{(D-2)}{2r}\left[2\left(1+\frac{2\mu b(r)}{r^3}\right)\left(1-\frac{b(r)}{r}\right)\Phi'-\frac{b(r)}{r^2}\left((D-3)+(D-5)\frac{\mu b(r)}{r^3}\right)\right], \tag{7}$$

$$\begin{aligned}p_t(r)=&\left(1+\frac{2\mu b(r)}{r^3}\right)\left(1-\frac{b(r)}{r}\right)\left[\Phi''+\Phi'^2+\frac{(b(r)-rb'(r))\Phi'}{2r(r-b(r))}\right]\\&+\left(\frac{b(r)-b'(r)r}{2r^2(r-b(r))}+\frac{\Phi'}{r}\right)\left(1-\frac{b(r)}{r}\right)\\&\times\left[(D-3)+(D-5)\frac{2\mu b(r)}{r^3}\right]\\&-\frac{b(r)}{2r^3}\left[(D-3)(D-4)+(D-5)(D-6)\frac{\mu b(r)}{r^3}\right]\\&-\frac{2\Phi'\mu}{r^4}(D-5)(b(r)-b'(r)r)\left(1-\frac{b(r)}{r}\right).\end{aligned} \tag{8}$$

Here, the prime symbolizes differentiation with respect to the radial coordinate r. The symbols $\rho(r)$, $p_r(r)$ and $p_t(r)$ represent the energy density, radial pressure and transverse pressure, respectively. In addition, we use the notation $\mu=(D-3)(D-4)\mu_1$ for the sake of convenience. Equations (6)–(8) comprise FEs, where one can see that there are five unknown quantities: $\rho(r)$, $p_r(r)$, $b(r)$, $p_t(r)$ and $\Phi(r)$. Thus, we need more conditions to evaluate all the unknowns. Here, a variety of approaches can be used to accomplish this analysis. In the next section, we consider various energy densities and analyze WH solutions.

3. Casimir WHs with electric charge

In 1948, the Casimir effect was first studied by Dutch physicist Hendrik Casimir [61]. It is possible that a force exists between parallel, uncharged, conducting surfaces. This is due to the consequence of disturbance induced by the vacuum of the electromagnetic field. The Casimir effect describes the plate distortion caused by the lowest energy state of a quantum electrodynamics vacuum, as proposed by Niels Bohr. The Casimir effect has been further validated by further experiments [62]. In quantum electrodynamics, the ground state (lowest energy state) is considered to be the main driving force for parallel, uncharged plates towards one another, due to the Casimir energy, which is rooted in classical quantum effects. The only artificial origin of exotic matter created in laboratories is the Casimir source. The structure of the boundaries affects how Casimir energy behaves [51]. The energy conditions, in particular the NEC ($\rho+p_r\geqslant 0$, $\rho+p_t\geqslant 0$), are not generally satisfied by exotic matter. Thus, it is logical to suppose that the exotic matter that exists in traversable WH, which inherently does not satisfy the NEC, is dependent on the Casimir effect. Employing an equation of state derived from Casimir energy, Garattini [51] introduced the idea of traversable WHs, these WHs are known as Casimir WHs.

3.1. Case A: Casimir WH with charge induced by parallel plates

The Casimir effect is characterized by a negative energy source that undergoes renormalization to yield a force of attraction between two plates. Representation of the force is given in equation (9)

$$\mathcal{E}(a)=-\frac{\hbar c\pi^2 A}{720a^3}. \tag{9}$$

In this case A stands for the surface area of the plates and a for their separation from one another. The energy linked with the Casimir energy density decays as the plates come together. The expression for energy density is written as follows:

$$\rho(a)=-\frac{\hbar c\pi^2}{720a^4}. \tag{10}$$

By taking into account the adjustment of the negative energy source through renormalization as shown in equation (9), the pressure can be calculated. The expression of pressure is

$$p(a)=-\frac{\mathrm{d}\mathcal{E}}{\mathrm{d}a}\times\left(\frac{1}{A}\right)=-\frac{\pi^2}{240}\times\left(\frac{1}{a^4}\right). \tag{11}$$

Further, we include the influence of an electromagnetic field created by a point charge in combination with the Casimir source [60]. The distance a between the plates is replaced by r. Thus, the total energy density is represented by

$$\rho=\rho_c+\rho_E=\frac{Q_1}{r^4}-\frac{l}{r^4}, \tag{12}$$

where

$$Q_1=\frac{Q^2}{2(4\pi)^2\epsilon_0}, \tag{13}$$

$$l=\frac{\pi^2}{720}. \tag{14}$$

In further analysis we will use $\hbar=c=1$ [63] unless otherwise stated. Now comparing, equation (41) and energy density defined in equation (12), we have the following equation:

$$\frac{1}{2r^6}[(D-2)(b(r)(2\mu rb'(r)+(D-4)r^3)+r^4b'(r)+(D-7)\mu b(r)^2)]=\frac{Q_1}{r^4}-\frac{l}{r^4}. \tag{15}$$

Confining our attention to $D=5$, and solving above differential equation, the obtained SF is written as follows:

$$b(r)=-\frac{r^3}{2\mu}\pm\frac{\sqrt{6h_1\mu r+4r(Q_1-l)\log(r)+\frac{3r^5}{2\mu}}}{6\sqrt{\frac{\mu}{r}}}, \tag{16}$$

where h_1 is an integration constant, which will be evaluated by taking $b(r_0)=r_0$, i.e.

$$h_1=\frac{2(l-Q_1)\log(r_0)+3(\mu+r_0^2)}{3\mu}. \tag{17}$$

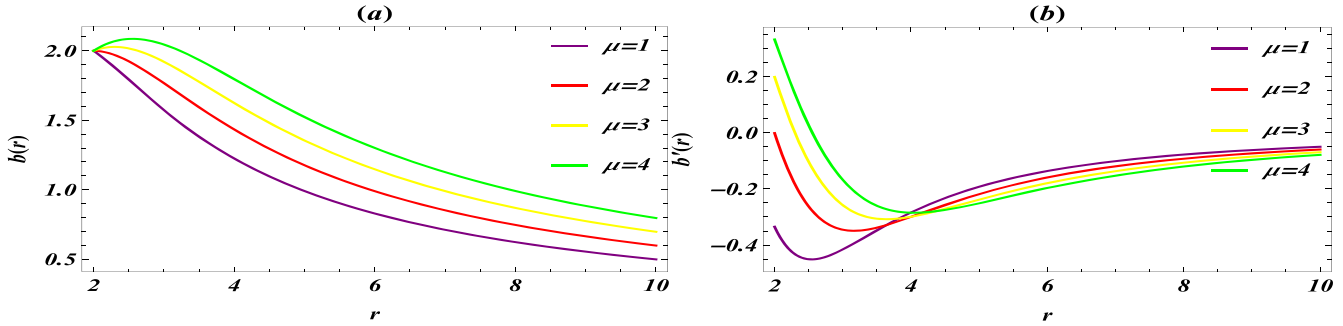

Figure 1. The left plots (a) reveal the behavior of $b(r)$ while the right plots (b) show the behavior of $b'(r)$ against r for a CCWH between two parallel plates. Herein, we set $r_0 = 2$, $Q = 0.25$ and $\epsilon_0 = 1$.

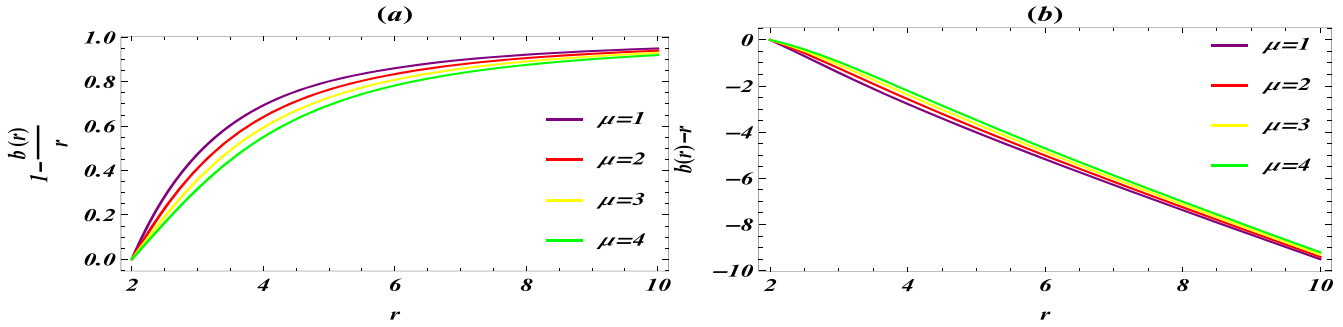

Figure 2. The left plots (a) reveal the behavior of $1 - b(r)/r$ while the right plots (b) show the behavior of $b(r) - r$ against r for a CCWH between two parallel plates.

The following is a description of final expression for the SF:

$$b(r) = -\frac{r^3}{2\mu} \pm \frac{\sqrt{\frac{3r^2}{2\mu} + 6r(r_0^2 + \mu) + 4r(-l + Q_1)\log\left(\frac{r}{r_0}\right)}}{6\sqrt{\frac{\mu}{r}}}. \tag{18}$$

Two unique SFs that correspond to the positive and negative signs are given in equation (18). We choose $b(r)$ with the positive sign which meets the the requirement for AF, i.e. $\frac{b(r)}{r} \to 0$ as $r \to \infty$. To study the WH conditions, the SF obtained in equation (18) is plotted graphically in figures 1 and 2, where figure 1(a) displays the behavior of the SF. It is seen that $b(r)$ is a growing function in terms of μ. Figure 1(b) shows $b'(r) < 1$, and this is satisfied for each value of μ. Figure 2(a) shows that SF is asymptotically flat, i.e. $1 - \frac{b(r)}{r} \to 1$ as $r \to \infty$. It can been observed that the AF condition is not satisfied for $\mu < 0$, but this is not displayed in plots. Figure 2(b) indicates the location of the WH throat.

In order to understand the behavior of electric charge Q with the SF, we kept μ constant in figure (3). Figure 3(a) shows that for all values of Q the SF decays. Figure 3(b) says that $b'(r) < 1$ for the whole domain of Q. We can see from figure 3(c) that the AF condition is fulfilled for the whole domain of Q.

The energy density of a CCWH between two plates placed in parallel is negative. The NEC is displayed in figure 4. It is clear that the NEC is not fulfilled, neither in the vicinity of the WH throat nor for distant regions from the throat. The ranges of parameters are also evaluated through regional plots, which are expressed as $\{\rho > 0$ for $50 < Q$ and $1 < \epsilon_0 < 10$, $\rho + p_r \geqslant 0$ for $50 < Q$ and $\mu < -5$, $\rho + p_t \geqslant 0$ for $0 < Q$ and $1 < \mu < 2\}$. Thus, NEC and WEC are violated, indicating the presence of exotic matter.

3.2. Case B: Casimir WH with charge induced by parallel cylinders

Cylinders which are placed in parallel can also generate the Casimir effect and are more workable for practical goals. In the present case, we have assumed two concentric cylinders of radius r_1 and r_2, with $r_2 > r_1$. Both cylinders are of length $\mathcal{L}$. The general form of the Casimir energy for the parallel cylinders is expressed as [64]

$$\mathcal{E}(r_1) = \frac{\pi^3 \mathcal{L}}{360 r_1^2 (\gamma - 1)^3}\left[1 + \frac{1}{2}(\gamma - 1) - \frac{1}{5\pi^2}(\gamma - 1)^2 + ...\right], \tag{19}$$

where $\gamma = \frac{r_2}{r_1}$. For short distances we take the limit $(\gamma - 1 \ll 1)$. The above relationship is reduced as follows:

$$\mathcal{E}(r_1) = -\frac{\pi^2 \mathcal{L}}{360 r_1^2 (\gamma - 1)^3}. \tag{20}$$

In this case we can find the energy density by using the feature that the volume between two concentric cylinders is $V = \pi(r_2 - r_1)\mathcal{L}$. Thus, we have

$$\rho = \frac{\mathcal{E}}{V} = \frac{\mathcal{E}}{\pi r_1^2 (\gamma^2 - 1)\mathcal{L}}. \tag{21}$$

The electromagnetic charge contributes to the Casimir effect observed between parallel cylinders: r_2 is replaced with r, and the whole expression is written as follows:

$$\rho = \frac{Q_1}{r^4} - \frac{r_1 l_2}{(r-r_1)^4(r_1+r)}, \tag{22}$$

where $l_2 = \frac{\pi^2}{360}$. Upon solving the differential equation for $D=5$ (by comparing equations (41) and (22)), we get the following expression for the SF:

$$\begin{aligned} b(r) = -\frac{r^3}{2\mu} \pm \frac{1}{(r_1-r)^2\sqrt{6(r_1+r)\frac{\mu}{r}}}\Bigg[\frac{r(r_1-r)^4(r_1+r)}{12} \\ \times\left(l_2\left(\frac{8r_1^3}{(r-r_1)^3}+\frac{30r_1^2}{(r_1-r)^2}+\frac{42r_1}{r-r_1}-3A\right)+48Q_1\log(r)\right) \\ +\left(6h_2\mu r+\frac{3r^5}{\mu}\right)(r_1-r)^4(r_1+r)\Bigg]^{\frac{1}{2}}, \end{aligned} \tag{23}$$

where $A = \log\left(\frac{r-r_1}{r+r_1}\right)$ and the constant of integration is h_2, which is estimated by $b(r_0)=r_0$, given by

$$\begin{aligned} h_2 = \frac{1}{72\mu(r_1-r_0)^3}[&20r_1^3l_2 - 54r_1^2l_2r_0 + 72r_1^3r_0^2 + 42r_1l_2r_0^2 \\ &- 216r_1^2r_0^3 + 216r_1r_0^4 - 72r_0^5 \\ &+ 72r_1^3\mu - 216r_1^2\mu r_0 + 216r_1\mu r_0^2 - 72\mu r_0^3 \\ &- 48Q_1(r_1-r_0)^3\log(r_0) + 3l_2(r_1-r_0)^3\log(r_0-r_1) \\ &- 3r_1^3l_2\log(r_1+r_0) + 9r_1^2l_2r_0\log(r_1+r_0) \\ &+ 3l_2r_0^3\log(r_1+r_0) - 9r_1l_2r_0^2\log(r_1+r_0)]. \end{aligned} \tag{24}$$

By putting in the value of h_2, we have the ultimate structure of the SF which is expressed as follows:

$$\begin{aligned} b(r) = -\frac{r^2}{12\mu}\Bigg[\sqrt{\frac{2\mu}{r^3(r_1-r)^4(r_1+r)}} \pm 6r\Bigg(r(r_1-r)^4(r_1+r)\Bigg(48Q_1\log(r)+\frac{18r^4}{\mu}+l_2(-3A \\ +\frac{-2r_1(10r_1^2-27r_1r+21r^2)}{(r_1-r)^3}\Bigg) \\ +\frac{1}{(r_1-r_0)^3}(20r_1^3l_2+72r_1^3r_0^2-54r_1^2l_2r_0-216r_1^2r_0^3+42r_1l_2r_0^2+216r_1r_0^4 \\ -72r_0^5+72r_1^3\mu-216r_1^2\mu r_0+216r_1\mu r_0^2-72\mu r_0^3-48Q_1(r_1-r_0)^3\log(r_0) \\ +3l_2(r_1-r_0)^3\log(r_0-r_1)+3l_2(r_1^3+3r_1^2r_0-3r_1r_0^2+r_0^3)\times\log(r_1+r_0))))^{1/2}]. \end{aligned} \tag{25}$$

Figures 5–8 display the evolution of the SF and other relevant properties. It is found that $b'(r) < 1, 1 - \frac{b(r)}{r} \to 1$ as $r \to \infty$ and $b(r) < r$ for different values of μ well as $\forall\, Q$. Moreover, we can observe in figure 8 that the NEC is not satisfied for the case of energy density between two parallel cylinders. We have determined the parameter ranges through regional plots, which are $\rho > 0$ for $70 < Q$ and $1 < \epsilon_0 < 1.5$, $\rho + p_r \geqslant 0$ for $0 < Q < 800$ and $\mu < -5$. We could not find any region for $\rho + p_t \geqslant 0$.

3.3. Case C: Casimir WH with charge induced by two spheres

We have considered another Casimir energy density system induced between two spheres with radius A, with the distance between them being represented by D_1. It has also been assumed that $D_1 \gg A$ by applying the multiple scattering method approach [65]. In the present scenario, ρ can be found by employing the result that the volume induced between two spheres is

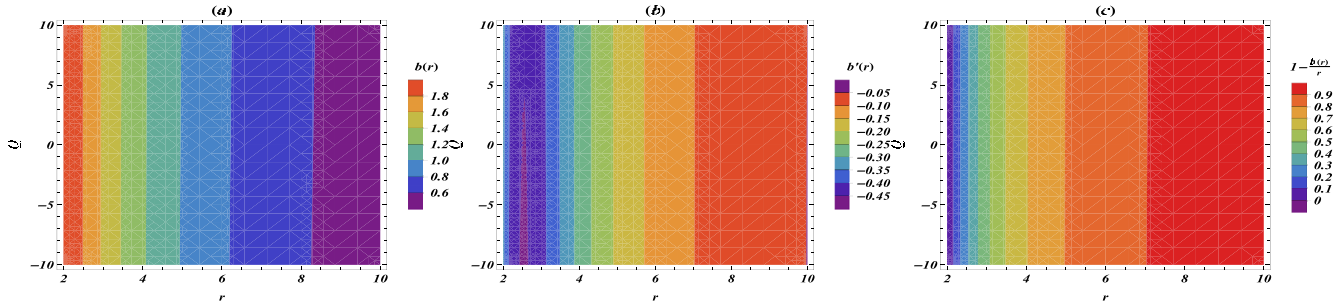

Figure 3. Contour plots illustrating $b(r)$, $b'(r)$ and $1-b(r)/r$ with respect to radial coordinate r are presented in (a), (b) and (c), respectively, for a CCWH situated between two parallel plates when $\mu = 1$.

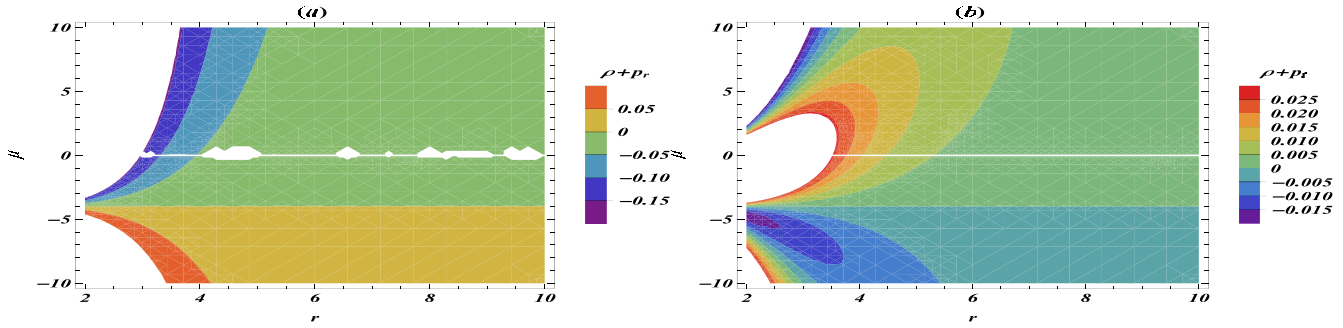

Figure 4. Contour plots depicting the NEC for a CCWH situated between two parallel plates.

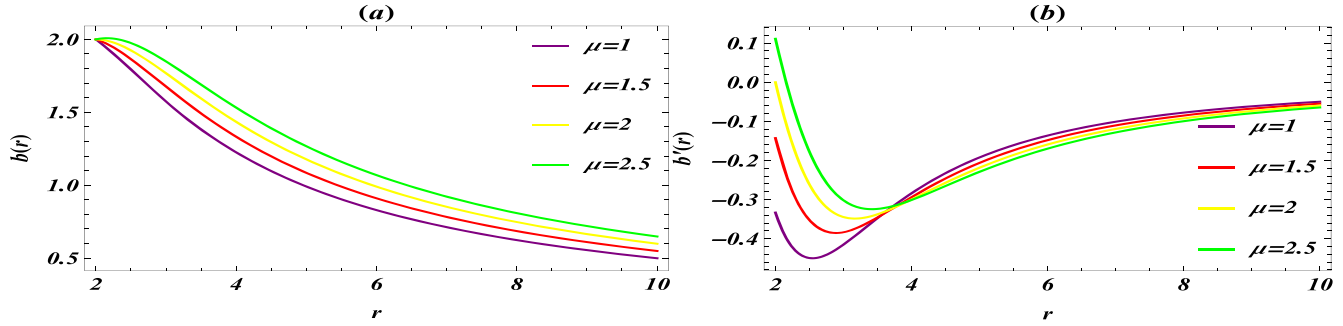

Figure 5. The left plots (a) reveal the behavior of $b(r)$ while the right plots (b) reveal the behavior of $b'(r)$ against r for a CCWH with energy density between the two parallel cylinders. Herein we set $r_1 = 0.1$.

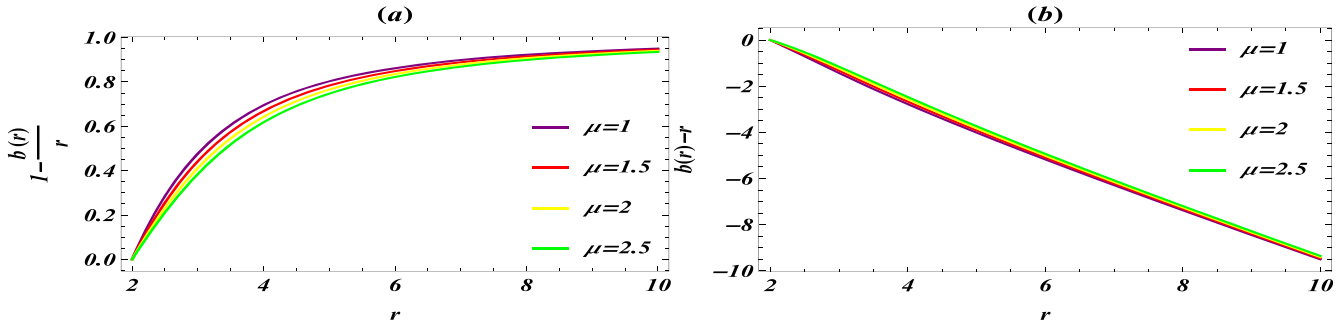

Figure 6. The left plots (a) reveal the behavior of $1-b(r)/r$ while right plots (b) reveal the behavior of $b(r)-r$ against r for a CCWH with energy density between the two parallel cylinders.

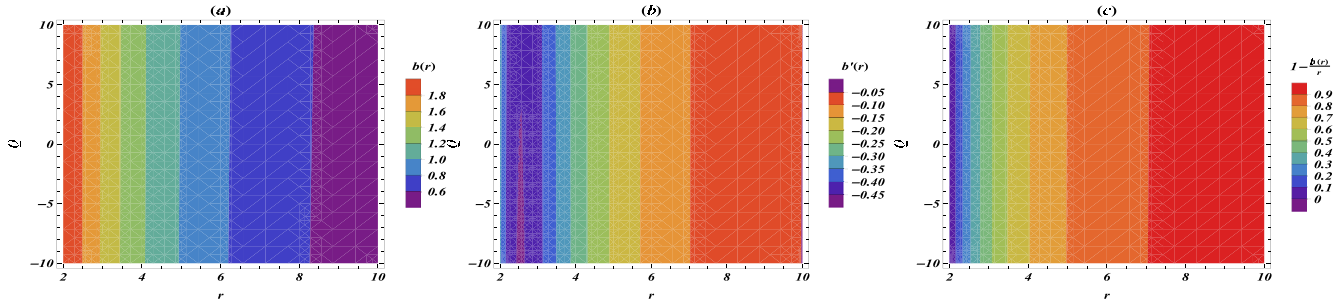

Figure 7. Contour plots illustrating $b(r)$, $b'(r)$ and $1-b(r)/r$ in terms of the radial coordinate r are presented in plots (a), (b) and (c), respectively, for a CCWH for the two parallel cylinders when $\mu = 1$.

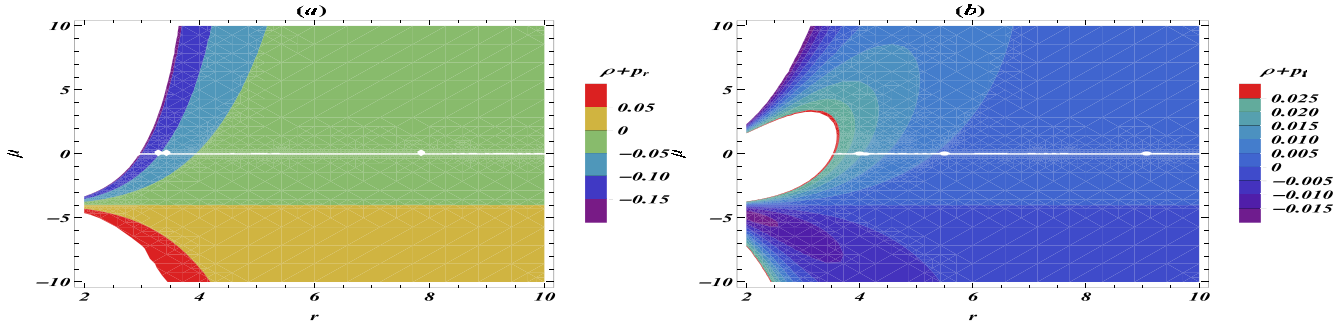

Figure 8. Contour plots illustrating the NEC for a CCWH positioned between two parallel cylinders.

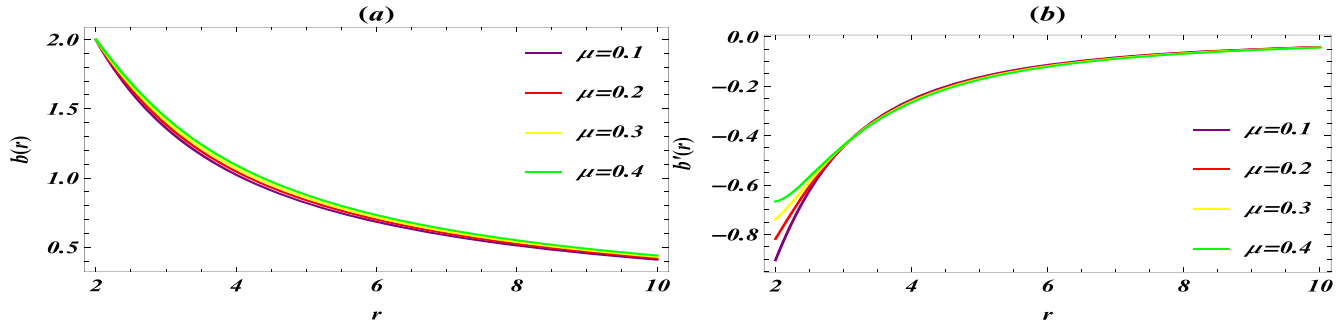

Figure 9. The left plots (a) reveal the behavior of $b(r)$ while the right plots (b) display the behavior of $b'(r)$ against r for a CCWH for the case of two spheres. Herein we set $A = 0.1$.

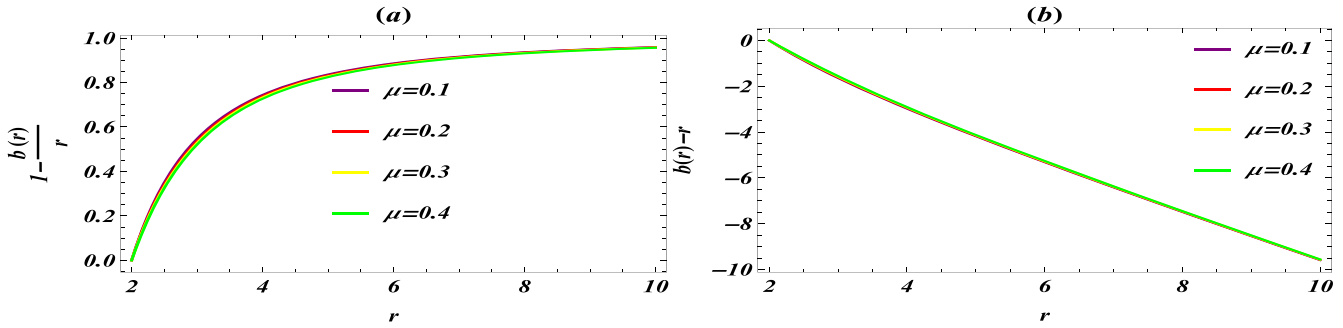

Figure 10. The left plots (a) reveal the behavior of $1-b(r)/r$ while the right plots (b) reveal the behavior of $b(r)-r$ against r for a CCWH for the case of two spheres.

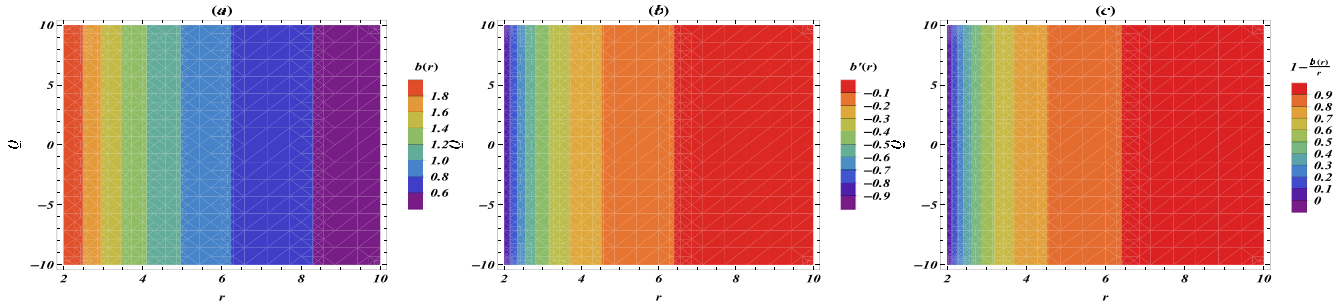

Figure 11. Contour plots illustrating $b(r)$, $b'(r)$, and $1-b(r)/r$ in terms of the radial coordinate r are presented in plots (a), (b), and (c), respectively, for CCWH for the case of the two spheres when $\mu=1$.

$V=\pi A^2 D_1$ (assuming $D_1 \gg A$). Thus, we have

$$\rho=\frac{\mathcal{E}}{\pi A^2 D_1}, \tag{26}$$

where

$$\mathcal{E}=-\frac{1}{8\pi D_1}\left[\frac{2A^2}{D_1^2}+\log\left(\frac{D_1^2}{D_1^2-4A^2}\right)+\frac{40A^4-6A^2D_1^2}{(D_1^2-4A^2)^2}\right]. \tag{27}$$

We note that in the case of two spheres the expression involves two variables A and D_1. To discuss this further, we will explore the Casimir effect by putting some restrictions on A and D_1. Next, we will assume $D_1=r$ and treat radius A as constant. The Casimir energy density in the presence of two spheres and electric charge is expressed as

$$\rho=\frac{Q_1}{r^4}-\frac{1}{8\pi^2A^2r^2}\times\left[\log\left(\frac{r^2}{r^2-4A^2}\right)+\frac{4(8A^6+6A^4r^2-A^2r^4)}{(r^3-4A^2r)^2}\right]. \tag{28}$$

By comparing equations (41) and (28) and employing a comparable procedure to the preceding sections, we get the ultimate form for $b(r)$

$$\begin{aligned}b(r)=&-\frac{r^3}{2\mu}\pm\frac{1}{2A\pi(4A^2-r^2)\sqrt{\frac{6\mu}{r}}}\\&\times\left[\frac{6\pi^2A^2r^5(4A^2-r^2)^2}{\mu}+2r(4A^2-r^2)^2\left(2A^2(4\pi^2Q_1-1)\log(r)+\frac{8A^4}{r^2-4A^2}\right.\right.\\&\left.-A^2\log(r^2-4A^2)+\frac{1}{2}r^2\log\left(\frac{r^2}{r^2-4A^2}\right)\right)\\&+\frac{r(4A^2-r^2)^2}{4A^2-r_0^2}(-4A^2(4\pi^2Q_1-1)(4A^2-r_0^2)\log(r_0)\\&+(4A^2r_0^2-r_0^4)\log\left(\frac{r_0^2}{r_0^2-4A^2}\right)\\&+2A^2(4(2A^2(6\pi^2(\mu+r_0^2)+1)-3\pi^2r_0^2(\mu+r_0^2))+(r_0^2-4A^2)\\&\left.\times\log(r_0^2-4A^2)))\right]^{1/2}.\end{aligned} \tag{29}$$

The WH constraints are checked in figures 9 and 10. For further analysis we have considered $b(r)$ with a plus sign as given in equation (29). Figure 9(a) displays the behavior of the SF, while figure 9(b) tells us that $b'(r)<1$. In figure 10(a), it is demonstrated that the AF condition is met. The plot for $b(r)-r$ is shown in figure 10(b), which locates the throat of the WH. We have plotted figure 11 to evaluate the behavior of electric charge on the SF. Figure 11(a) shows that the SF is a decaying function of Q for all domains of Q. The condition $b'(r)<1$ is met, and the AF condition is satisfied for the parameter Q as shown in figures 11(b) and (c), respectively.

We can observed from figure 12 that $\rho+p_r\leqslant 0$ for $\mu>0$ and $\rho+p_t\leqslant 0$ for $\mu<0$. $\rho+p_r\geqslant 0$ for $\mu<0$ and $\rho+p_r\geqslant 0$ for $\mu>0$, thus the NEC is not satisfied. We have determined the parameter ranges through regional plots which are $\rho+p_r\geqslant 0$ for $Q>0$ & $\mu<-5$. We are unable to identify any region for $\rho\geqslant 0$ and $\rho+p_t\geqslant 0$, therefore NEC is not satisfied.

3.4. Case D: charged Casimir GUP-corrected WH

The concept of minimal length introduces a modification to the uncertainty principle within the framework of quantum mechanics. The connection between the uncertainty principle and minimal length becomes a fascinating path for

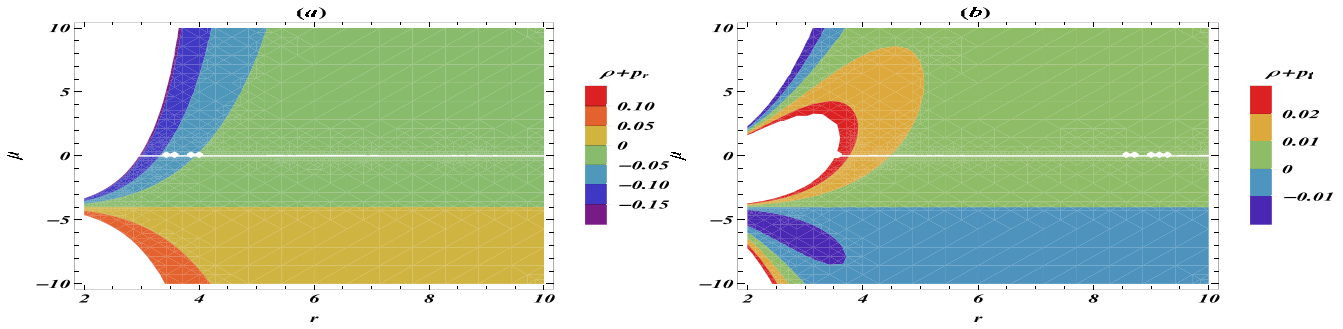

Figure 12. Contour plots showcasing the NEC for a CCWH situated between two parallel cylinders.

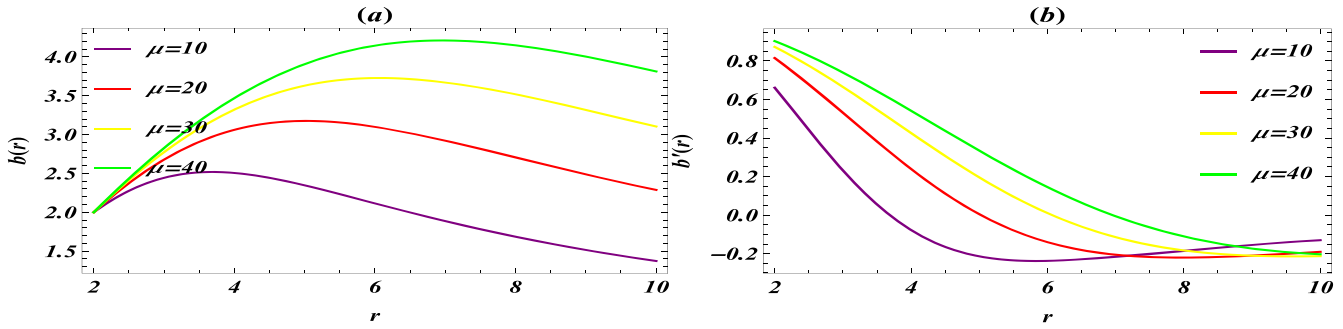

Figure 13. The left plots (a) reveal the behavior of $b(r)$ while the right plots (b) reveal the behavior of $b'(r)$ against r for a charged GUP-corrected WH for ζ_1. Herein we set $\alpha = 2$ and $Q = 0.5$.

exploration, providing insights into the intricate connections between quantum theory and the geometric structure of the cosmos. In addition, issues of the GUP concerned with examination of the momentum and position are studied in [66, 67]. Our objective is to discern the influence of the GUP on the Casimir effect. We have observed that to understand the physical phenomena, momentum and position must be conjugate variables for each other. We are unable to consider the position eigenspace as a representation of the actual physical position because of its modification to the position–momentum relation. The states projected onto the maximally localized state, often known as the 'quasi position representation', is an alternative method of discussing the position that is covered in [66]. The physical position states, also referred to as 'maximally localized states', can be obtained principally in two ways. One method is the canonical approach suggested by Kempf, Mangano and Mann (KMM) [66]. However, Detournay, Gabriel and Spindel (DGS) [67] later found that this method does not yield all the squeezed states, which are the 'maximally localized states'. To locate these states, they therefore used a variational algorithm. In this article, we have considered a method to find the influence on a CCWH. In N-dimensional minimal length the restated commutation relation is interpreted as in equation (30) [68]

$$[x_i, p_j] = i[g(p^2)p_i p_j + f(p^2)\delta_{ij}], \quad i, j = 1, 2, 3 \ldots N. \tag{30}$$

Here $f(p)$ and $g(p)$ denote generic functions. By using the rotational and translational invariance of the commutation relation, one may determine this. Selecting various generic functions enables maximum localized states and results in distinct models. We will now discuss two distinct GUP approaches, KMM [66] and DGS [67]. The KMM method employs the compressed state and the DGS method uses the variational principle. The number of dimensions of the specific model under consideration determine the specific form of these states. According to [69], the generalized functions $f(p^2)$ and $g(p^2)$ are key components of the KMM model. Here, we have

$$f(p^2) = \frac{\alpha p^2}{\sqrt{1 + 2\alpha p^2} - 1}, \quad g(p^2) = \alpha. \tag{31}$$

The maximally localized states for the KMM model demands

$$k_i = \left[\frac{\sqrt{1 + 2\alpha p^2} - 1}{\alpha p^2}\right] p_i, \tag{32}$$

$$w(p) = \left[\frac{\sqrt{1 + 2\alpha p^2} - 1}{\alpha p^2}\right], \tag{33}$$

$$\omega(p) = \left[\frac{\sqrt{1 + 2\alpha p^2} - 1}{\alpha p^2}\right]^{\gamma/2}, \tag{34}$$

In the above equations, α represents the parameter for minimal uncertainty while γ is expressed as $\gamma = 1 + \sqrt{1 + N/2}$, where N denotes the number of spatial dimensions. The construction of maximally localized states for the DGS method requires certain conditions expressed as follows:

$$k_i = \left[\frac{\sqrt{1 + 2\alpha p^2} - 1}{\alpha p^2}\right] p_i, \tag{35}$$

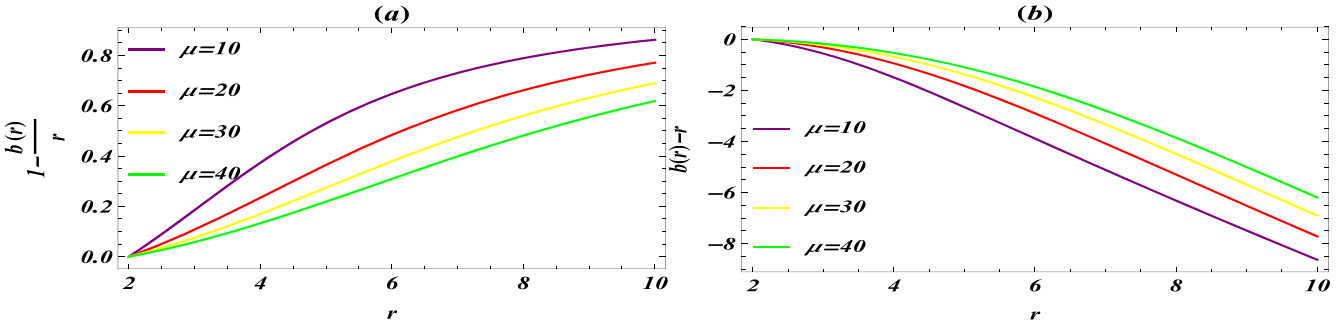

Figure 14. The left plots (a) reveals the behavior of $1-b(r)/r$ while the right plots (b) reveal the behavior of $b(r)-r$ against r for a charged GUP-corrected WH for ζ_1.

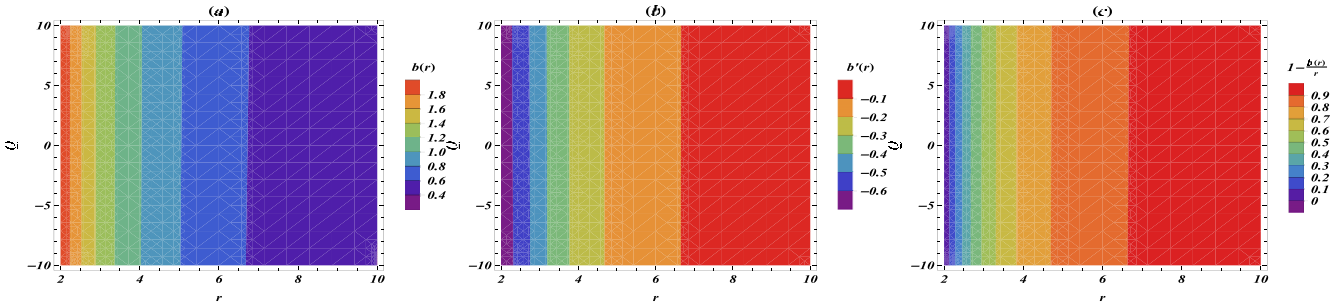

Figure 15. Contour plots illustrating $b(r)$, $b'(r)$ and $1-b(r)/r$ in terms of the radial coordinate r are presented in plots (a), (b) and (c), respectively, for a charged GUP-corrected WH for ζ_1 when $\mu=10$.

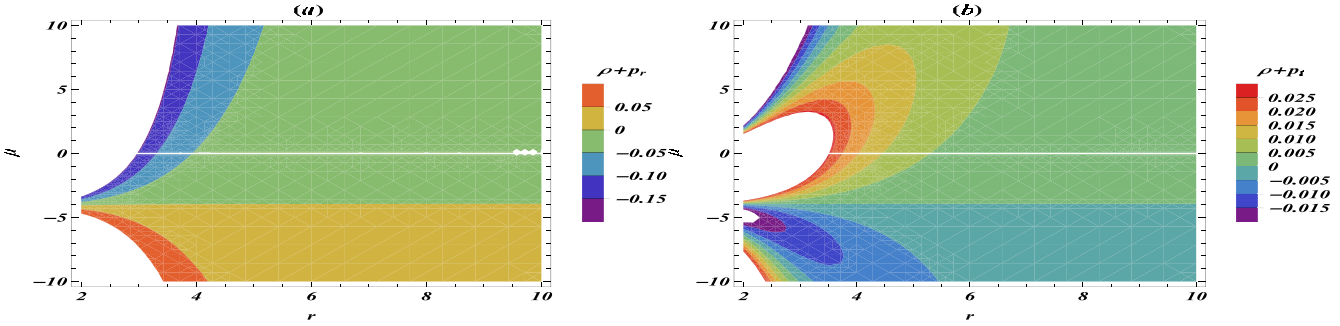

Figure 16. Contour plots illustrating the NEC for a CCWH with GUP corrections, specifically for the parameter ζ_1.

$$w(p)=\left[\frac{\sqrt{1+2\alpha p^2}-1}{\alpha p^2}\right], \tag{36}$$

$$\omega(p)=\frac{\sqrt{2}}{\pi}\left[\frac{\sqrt{1+2\alpha p^2}-1}{\alpha p^2}\right]^{\beta/2} \times \sin\left[\frac{\sqrt{2}\pi\sqrt{1+2\alpha p^2}-1}{2\sqrt{\alpha p^2}}\right]. \tag{37}$$

The objective of the GUP and minimal length idea is to obtain the limited energy induced inside the uncharged plates. This idea was presented by Frassino and Panella. They developed the Hamiltonian and determined the Casimir energy modifications imposed by the presence of a minimal length. The Casimir energy of the two cases, which is used for the construction of maximally localized states, is written as [68]

$$\mathcal{E}(a)=-\frac{\pi^2 A}{720a^3}\left(1+\zeta_i\frac{\alpha}{a^2}\right), \tag{38}$$

where

$$\zeta_1=\pi^2\left[\frac{28+3\sqrt{10}}{14}\right], \tag{39}$$

$$\zeta_2=4\pi^2\left[\frac{3+\pi^2}{21}\right]. \tag{40}$$

The energy densities and pressure, according to the model presented, become the following:

$$\rho(a)=-\frac{\pi^2}{720a^4}\left(1+\zeta_i\frac{\alpha}{a^2}\right), \tag{41}$$

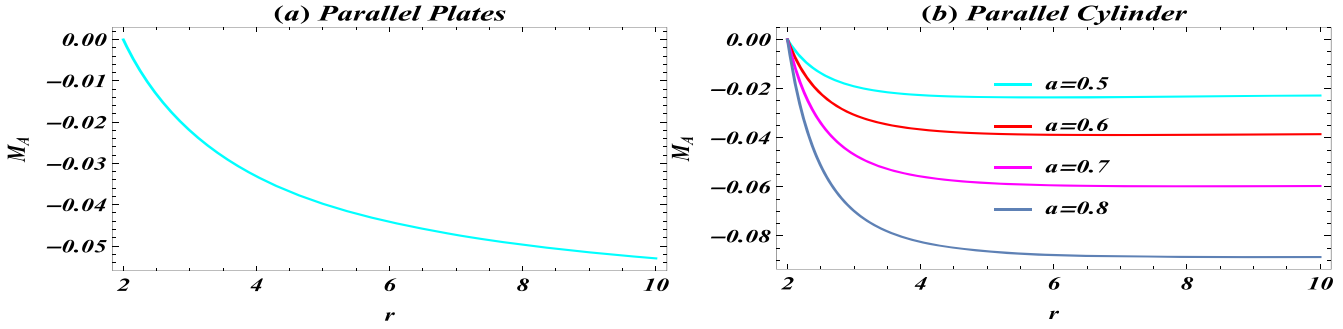

Figure 17. The left plot (a) shows M_A of a WH from parallel plates while the right plots (b) show M_A of a WH from parallel cylinders. Herein we set $r_0 = 2$, $\epsilon_0 = 0.5$ and $Q = 0.5$.

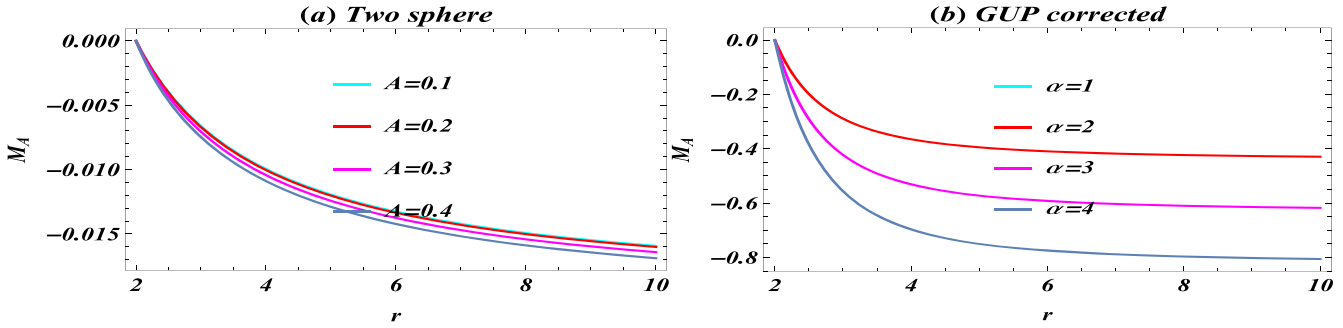

Figure 18. The left plots (a) display M_A of a WH from two spheres while the right plots (b) show M_A of a WH from GUP correction.

$$p(a) = -\frac{\pi^2}{720a^4}\left(1 + \frac{5\zeta_i}{3}\frac{\alpha}{a^2}\right), \tag{42}$$

where $i = 1,\ 2$ represent KMM and DGS models, respectively.

The energy density of a GUP-corrected WH with electric charge is expressed as

$$\rho = \frac{Q_1}{r^4} - \frac{l\left(\frac{\alpha\zeta_i}{r^2} + 1\right)}{r^4}. \tag{43}$$

By comparing energy densities expressed in equations (41) and (43), we have the ultimate structure for the SF, written as follows:

$$b(r) = -\frac{r^3}{2\mu} \pm \frac{\sqrt{\frac{3r^5}{2\mu} + 6r(r_0^2 + \mu) + 2l\zeta_i\alpha r\left(\frac{1}{r^2} - \frac{1}{r_0^2}\right) + 4r(-l + Q_1)\log\left(\frac{r}{r_0}\right)}}{\sqrt{\frac{6\mu}{r}}}. \tag{44}$$

We have chosen $b(r)_+$ because it satisfies the asymptotically flat constraint. The WH conditions are discussed graphically and analytically by employing the KMM method which is represented by ζ_1. The conditions for a GUP-corrected WH are plotted in figures 13 and 14.

- The behavior of $b(r)$ can be seen from figure 13(a). Near the WH throat it is an increasing function of r, while it decreases away from the throat. Figure 13(b) shows that $b'(r) < 1$, and it can be analyzed that for larger values of μ this condition is not satisfied. Figure 14(a) is plotted for the AF condition which says that $1 - \frac{b(r)}{r} \to 1$ as $r \to \infty$ and $\mu = 10$. For higher values of μ, the SF is no longer asymptotically flat. Moreover, the AF condition is also not satisfied for $\mu < 0$. Figure (14)(b) depicts the throat point.
- The plot in figure 15(a) shows that charged GUP-corrected $b(r)$ is a decaying function of Q when $\mu = 10$. Figure 15(b) shows that for $Q > 0$, $Q < 0$ and $Q = 0$, $b'(r) < 1$. In figure 15 (c) we can see that for $Q > 0$, $Q < 0$ and $Q = 0$ the AF condition is satisfied.
- Figure 16 shows contour plots of the NEC for a CCWH with GUP correction, specifically for the parameter ζ_1. We can see that the NEC is not valid as $\rho + p_r \geqslant 0$ for $\mu \leqslant -4$ while $\rho + p_t \geqslant 0$ for $\mu \geqslant -4$. ρ is negative, therefore, NEC and WEC are not satisfied. This suggests the existence of exotic matter and the presence of a WH. The ranges of parameters are $\rho > 0$ for $\alpha < 0$, $Q > 0$, $\rho + p_r > 0$ for $Q > 0$ & $\mu < -5$, $\rho + p_r > 0$ for $Q > 0$ & $1 < \mu < 2$. In short, we could not find a common region for which conditions could hold, therefore, both the NEC and WEC are not satisfied.

4. Active gravitational mass in a CCWH

The gravitational mass within the space from the throat r_0 to the radius r can be found by employing the following relation:

$$M_{\mathcal{A}} = \int_{r_0}^{r} (\rho(r) r^2) \mathrm{d}r, \tag{45}$$

where $M_{\mathcal{A}}$ represents the gravitational mass. Utilizing the energy density from each given scenario, we will assess the mass as a function of radius. This mass quantifies the intensity of the gravitational flux surrounding an object. The gravitational mass function for case A is written as

$$M_{\mathcal{A}} = -\frac{(2\pi^4\epsilon_0 - 45Q)(r - r_0)}{360\pi r r_0 \epsilon_0}. \tag{46}$$

The expression for the gravitational mass in case B is given by

$$M_{\mathcal{A}} = \frac{1}{4320\pi\epsilon_0}\left[-\frac{\pi^4\epsilon_0(2a(2a^2 - 3ar_0 - 3r_0^2) + 3(a - r_0)^3\log(r_0 - a) - 3(a - r_0)^3\log(a + r_0))}{a(a - r_0)^3} + \frac{540Q}{r_0}\right.$$
$$\left. - \frac{540Q}{r} + \frac{\pi^4\epsilon_0(2a(2a^2 - 3ar - 3r^2) + 3(a - r)^3\log(r - a) - 3(a - r)^3\log(a + r))}{a(a - r)^3}\right]. \tag{47}$$

The active gravitational mass (AGM) $M_{\mathcal{A}}$ in case C is formulated as

$$M_{\mathcal{A}} = \frac{1}{8\pi A^2\epsilon_0}\left[\frac{A^2Q(r^2 - 4A^2) + 4\epsilon_0\left(8A^4 - 4A^2r^2 + (r^4 - 4A^2r^2)\log\left(\frac{r^2}{r^2 - 4A^2}\right)\right)}{4A^2r - r^3}\right.$$
$$\left. - \frac{A^2Q(r_0^2 - 4A^2) + 4\epsilon_0\left(8A^4 - 4A^2r_0^2 + (r_0^4 - 4A^2r_0^2)\log\left(\frac{r_0^2}{r_0^2 - 4A^2}\right)\right)}{4A^2r_0 - r_0^3}\right]. \tag{48}$$

The expression for the AGM $M_{\mathcal{A}}$ in case D is stated as

$$M_{\mathcal{A}} = -\frac{\pi\left(42r^2r_0^2\left(\pi^2 - \frac{45Q}{2\pi^2\epsilon_0}\right)(r - r_0) + \pi^4(3\sqrt{10} + 28)\alpha(r^3 - r_0^3)\right)}{7560r^3r_0^3}. \tag{49}$$

In this part of manuscript, we study the $M_{\mathcal{A}}$ of WHs constructed in the previous sections. The presence of a negative AGM serves as an indicator of the existence of exotic matter. Notably, the Casimir effect emerges as a tangible manifestation of such exotic matter in the background of theoretical physics. The Casimir effect contributes to the negativity observed in the plotting of gravitational mass, influencing the gravitational properties of the surrounding space. This phenomenon emphasizes the interplay between theoretical concepts, such as the Casimir effect and the gravitational characteristics of the cosmic result. We have plotted $M_{\mathcal{A}}$ for each case in figures 17 and 18 for constant Q. We observe that $M_{\mathcal{A}}$ is negative for each WH. In each case with increasing value of a, A and α, $M_{\mathcal{A}}$ decreases. In figure 19, when the electric charge is increasing, M_A increases. However, for a WH developed from two spheres $M_{\mathcal{A}}$ decreases with the increase in electric charge. $M_{\mathcal{A}}$ decays with increase in Q for a GUP-corrected WH. Figure 20 explains the dynamics of the active gravitational mass for both the two-sphere and GUP-corrected scenarios, considering different charge values.

5. Embedding diagram of charged Casimir WHs

The purpose of this section is to gain a deep knowledge of WH geometry. In this analysis, we consider the WH spacetime described by the expression in equation (5). Now we consider $t =$ constant and $\theta = \pi/2$, and obtain an equatorial segment for this kind of WH metric. Thus, this metric can be written as

$$\mathrm{d}s^2 = \left(1 - \frac{b(r)}{r}\right)^{-1}\mathrm{d}r^2 + r^2\mathrm{d}\phi^2. \tag{50}$$

Utilizing the WH metric at hand, we will proceed to generate both 2D and 3D embedding diagrams, depicting the surface and spatial aspects, respectively. Consequently, we will denote cylindrical coordinates as (z, r, ϕ). The depiction of the embedding metric is outlined as follows:

$$\mathrm{d}s^2 = \mathrm{d}z^2 + \mathrm{d}r^2 + r^2\mathrm{d}\phi^2. \tag{51}$$

The axial symmetry of the embedded surface can be utilized to demonstrate the relationship $z = z(r)$. The surface's line

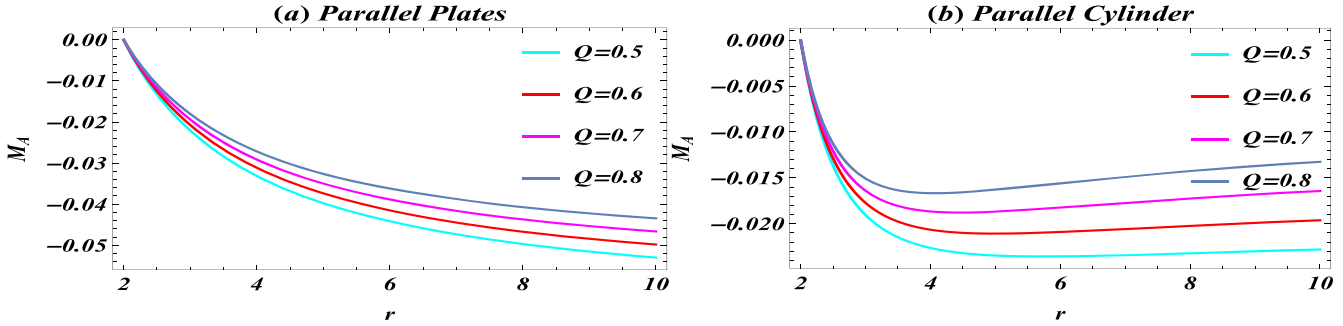

Figure 19. The left plots (a) display M_A of a WH from parallel plates while the right plots (b) shows M_A of a WH from parallel cylinders. The value of other parameters is a=0.5.

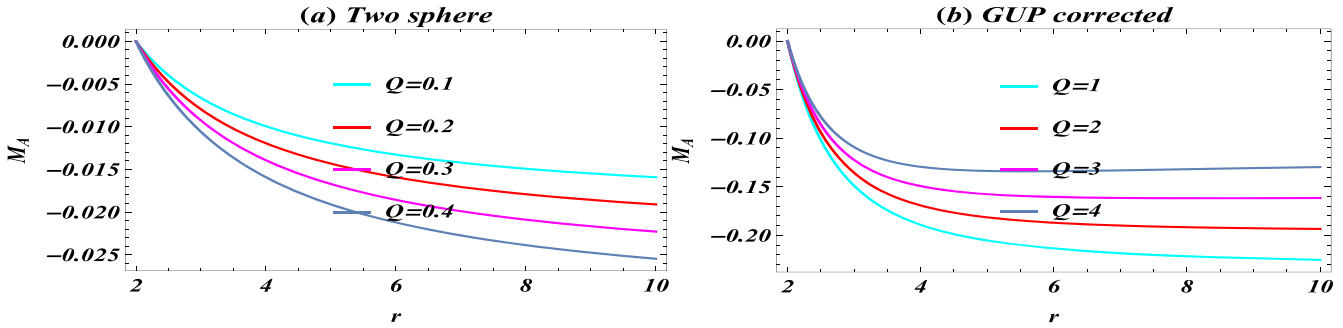

Figure 20. The left plots (a) display M_A of a WH from two spheres while the right plots (b) show M_A of a WH from the GUP-corrected energy density. The selected values of parameters are $A = 0.1$ and $\alpha = 1$.

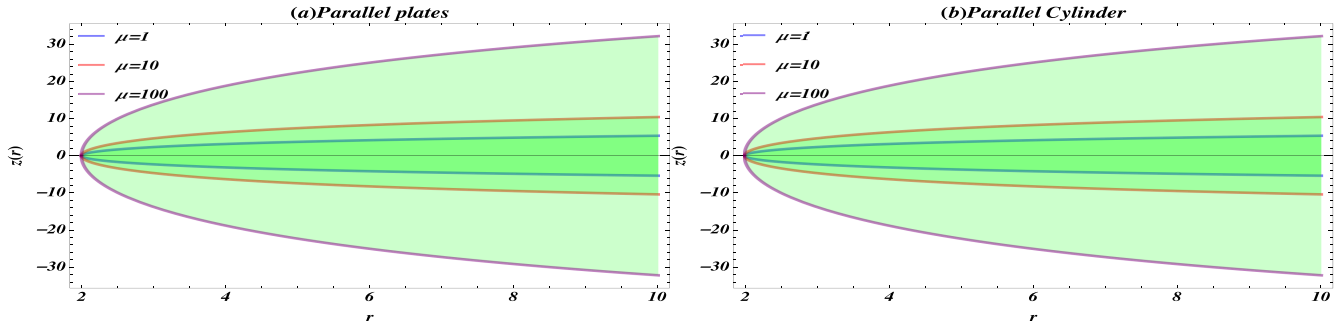

Figure 21. 2D visualization of $z(r)$ for a CCWH for cases A (left) and B (right).

element is stated as follows:

$$ds^2 = \left(1 + \left(\frac{dz}{dr}\right)^2\right)dr^2 + r^2 d\phi^2. \tag{52}$$

By equating equation (50) with equation (52), we obtain

$$\frac{dz}{dr} = \pm\left(\frac{b(r)}{r - b(r)}\right)^{1/2}. \tag{53}$$

The function $b(r)$ produced from the CCWH as explained in equation (18) will be used in this situation.

The embedding diagram showing the top universe ($z > 0$) and bottom universe ($z < 0$) of the Casimir WH is shown in figure 21, where the plot reveals that by growing the value of the GB-coupled parameter the WH expands. Figure 22 displays the 2D visualization of $z(r)$ for a CCWH, while left plot is for case C and right plot is for case D. The 3D embedding plot view is the same for all the cases, therefore we have given a 3D visualization for different domains of r in figure 23. In figure 23 the left trajectory has domain $2 < r < 3$, the middle one has $2 < r < 10$ and right has domain $2 < r < 1000$. The observed behavior suggests AF, which is defined as $\frac{dz}{dr} \to 0$ as $r \to \infty$ when one moves far away from the WH throat.

6. Behavior of the CF on charged Casimir WHs

Within the framework of self-gravitating, static and spherically symmetric systems in GR, Herrera [43] introduced the idea of the CF in 2018. The CF mostly applies to systems with homogeneous energy density and isotropic pressure,

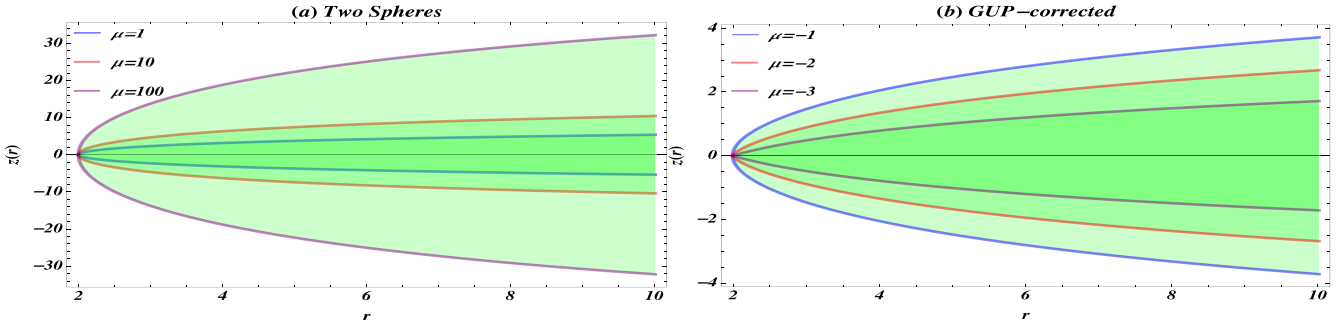

Figure 22. 2D visualization of $z(r)$ for a CCWH for cases C (left) and D (right).

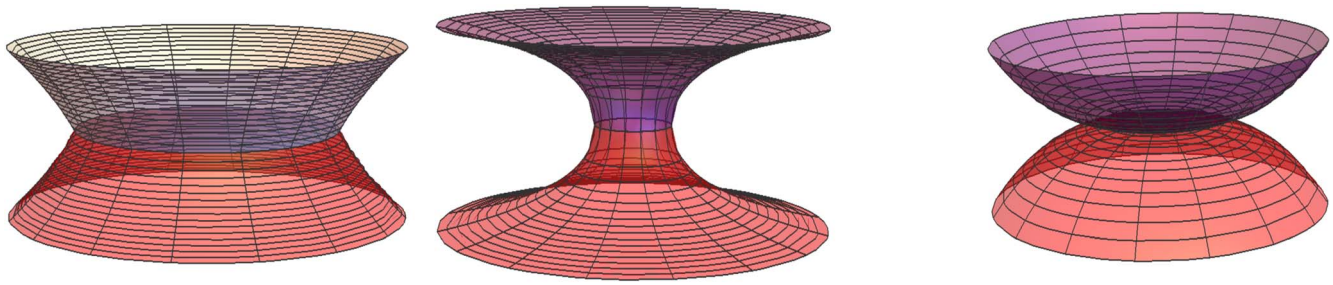

Figure 23. The dynamics of entire surface visualization for a CCWH are produced by rotating the embedded curve about the vertical z axis. Here $\mu = 100$.

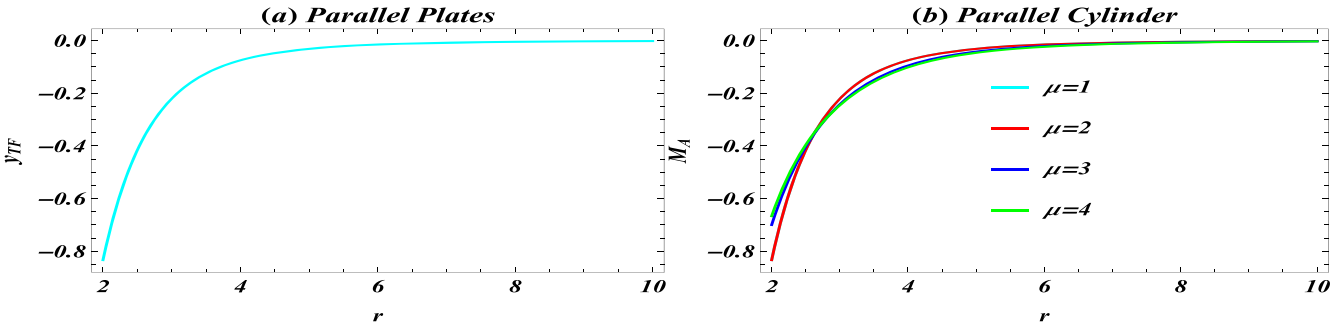

Figure 24. The left plot (a) reveals the CF of a CCWH induced between two parallel plates while the right plots (b) show the CF of a CCWH induced between two parallel cylinders.

indicative of simple or minimally complicated properties. The CF has a value of zero in such fluid distributions. The CF may also be zero in self-gravitating systems with anisotropic pressure and inhomogeneous energy density if the influence of these two components on the CF is completely negligible. For static spherically symmetric spacetimes, CF denoted by $\mathcal{Y}_{TF}$ has the following expression:

$$\mathcal{Y}_{TF} = \Pi - \frac{1}{2r^3}\int_{r_0}^{r} r^3 \frac{\mathrm{d}\rho(r)}{\mathrm{dr}}\mathrm{dr}, \tag{54}$$

where $\Pi = p_r - p_t$. For $D = 5$ and constant RSF.

The behavior of the CF can be observed from figures 24 and 25 for each scenario. $\mathcal{Y}_{TF}$ is seen to lie within a defined range, namely $-1 < \mathcal{Y}_{TF} \leqslant 0$, which is dependent on the values of μ and Q. Additionally, it is noticed that $\mathcal{Y}_{TF}$ tends towards zero as the radial distance r approaches infinity or moves away from the WH throat. Hence, in the neighborhood of the WH throat, the value of $\mathcal{Y}_{TF}$ increases, while for high values of r, $\mathcal{Y}_{TF} \to 0$.

7. Equilibrium forces for a charged Casimir WH

The SF developed for different cases of a CCWH in EGB gravity will be used in this section to determine the different forces. Here, we consider the generalized TOV equation, which is written as

$$-\frac{\mathrm{dp}_r}{\mathrm{dr}} - \frac{\Phi'(r)}{2}(\rho + p_r) - \frac{2}{r}(p_r - p_t) = 0, \tag{55}$$

where

$$\mathcal{F}_g = -\frac{\Phi'(r)}{2}(\rho + p_r), \tag{56}$$

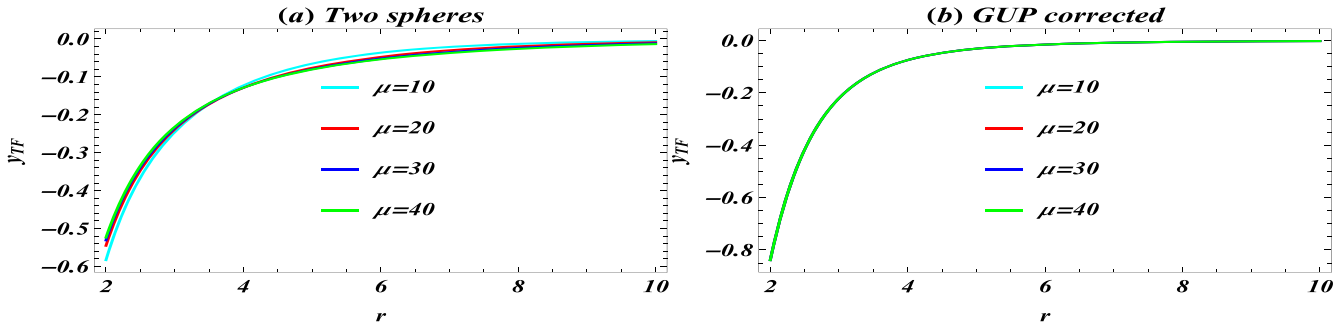

Figure 25. The left plots (a) reveal the CF of a CCWH induced between two spheres while the right plots (b) show the CF of a charged GUP-corrected WH.

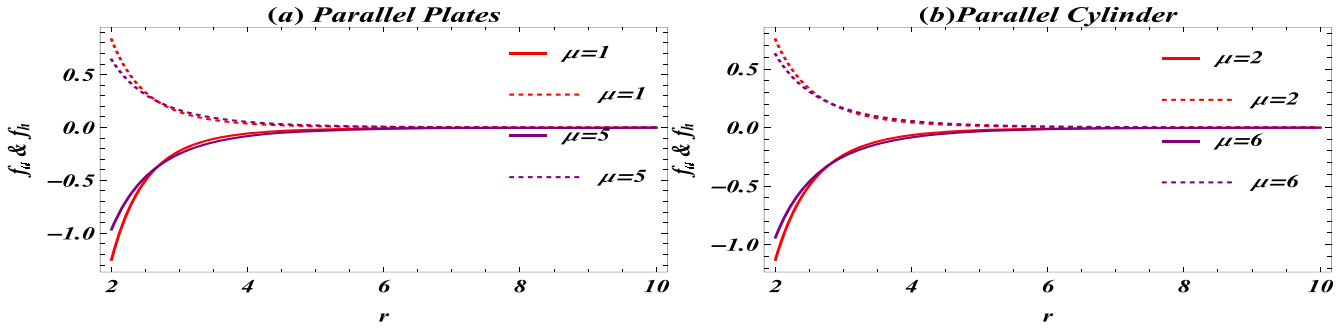

Figure 26. The left plots (a) reveal the equilibrium configuration of a CCWH due to two parallel plates while the right plots (b) display the equilibrium configuration of a CCWH due to two parallel cylinders. The values of the other parameters are $Q = 0.25$, $a = 1$ and $\epsilon_0 = 1$.

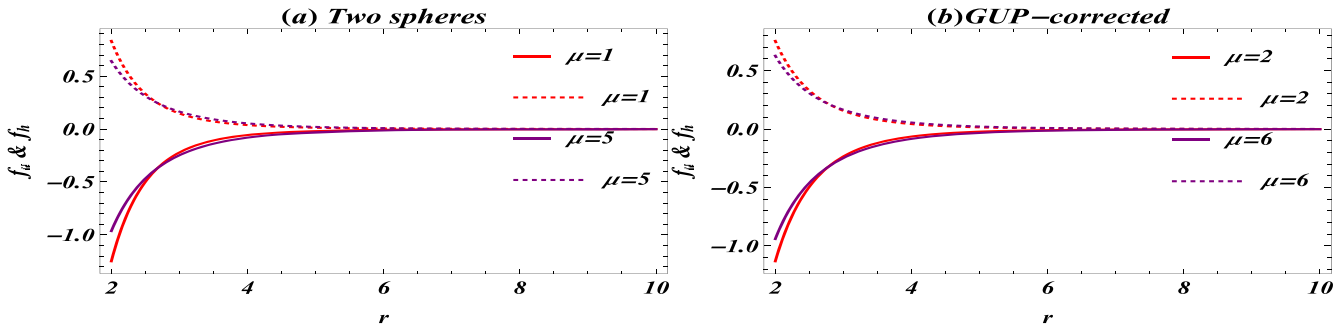

Figure 27. The left plots (a) reveal the equilibrium configuration of a CCWH due to two spheres while the right plots (b) display the equilibrium configuration of a charged GUP-corrected Casimir WH. The values of the other parameters are $Q = 0.25$, $A = 0.1$ and $\epsilon_0 = 1$.

$$\mathcal{F}_h = -\frac{\mathrm{dp}_r}{\mathrm{dr}}, \tag{57}$$

$$\mathcal{F}_a = -\frac{2}{r}(p_r - p_t). \tag{58}$$

Here, the terms $\mathcal{F}_g$, $\mathcal{F}_h$ and $\mathcal{F}_a$ stand for the gravitational, hydrostatic and anisotropic forces, respectively. The sum of these forces must be equal to zero for the system to be in equilibrium. The equilibrium requirement in the present situation is reduced to $\mathcal{F}_h + \mathcal{F}_a = 0$. These forces are computed and presented in the following graphs utilizing SFs that have been constructed in other sections.

Figures 26 and 27 display the behavior of hydrostatic and anisotropic forces for various values of μ. Figure 26(a) reveals the behavior of $\mathcal{F}_h$ and $\mathcal{F}_a$ with varying μ for a CCWH between two parallel plates. Figure 26(b) exhibits the behavior of $\mathcal{F}_h$ and $\mathcal{F}_a$ with varying μ for a CCWH between two parallel cylinders. Similarly, the aforementioned forces are displayed for two spheres and are GUP-corrected in figure 27. We have observed that forces cancel the effects of each other for $\mu = 1$ and $\mu = 5$ in the scenario of parallel plates and two spheres. However, in the scenario of parallel cylinders and GUP correction we have seen that forces cancel the influences of each other for $\mu = 2$ and $\mu = 6$. Further, it has been observed that for $r > 6$ these forces completely balance each other's effects.

8. Summary

The EGB theory is a modified gravity theory that includes higher-order curvature corrections and may provide insights

Table 1. Ranges of parameters for WEC.

WH	WEC/NEC
Case A	$\rho > 0$ for $50 < Q$ and $1 < \epsilon_0 < 10$, $\rho + p_r \geqslant 0$ for $50 < Q$ and $\mu < -5$, $\rho + p_t \geqslant 0$ for $0 < Q$ and $1 < \mu < 2$
Case B	$\rho > 0$ for $70 < Q$ and $1 < \epsilon_0 < 1.5$, $\rho + p_r \geqslant 0$ for $0 < Q < 800$ and $\mu < -5$
Case C	$\rho + p_r \geqslant 0$ for $Q > 0$ and $\mu < -5$
Case D	$\rho > 0$ for $\alpha < 0$, $Q > 0$, $\rho + p_r > 0$ for $Q > 0$ and $\mu < -5$, $\rho + p_r > 0$ for $Q > 0$ and $1 < \mu < 2$,

into the behavior of gravity in high-energy regimes. On the other hand, the theory of Casimir energy is based on the quantum effect, which says that the initial state of quantum electrodynamics is the main factor that causes parallel, uncharged plates to attract. Moreover, it is the sole known source of exotic matter that can be generated in laboratory settings. The shape and geometry of the boundaries have a significant impact on the Casimir energy, and it has been observed that exotic matter, including Casimir energy, frequently violates energy conditions, particularly the NEC. It is logical to assume that the Casimir effect in traversable WHs also violates the NEC due to the presence of exotic matter. Garattini proposed the concept of traversable WHs using an equation of state derived from Casimir energy and known as Casimir WHs [51]. By exploring the implications of the EGB theory for Casimir energy and traversable WHs, we may uncover new insights into the behavior of gravity and the structure of spacetime.

Research into the charged Casimir effect within the framework of WH spacetime in the background of EGB gravity is the primary subject of this article. Four distinct systems that closely resemble the actual image of the WH are chosen. In [60] Garattini continued his search for the equation which connects Casimir energy and the traversability of a WH. He took into account both the potential negative energy density produced by a Casimir source as well as the influence of an electromagnetic field created by an electric charge. This merger adds a new definition of an electrovacuum source that includes a parameter related to the throat size. The present article covers four different Casimir energy density systems since the goal of the research is to explore the effects of an electric charge on a Casimir WH.

- We assumed energy densities between parallel plates, cylinders and spheres and due to the GUP-corrected function. To find out the SF we compared the energy density of EGB gravity and that due to the charged Casimir source. Ultimately, we graphically examined the $b(r)$ derived for each system. We noticed that under the asymptotic background, the $b(r)$ we obtained meet the flare-out criterion. Also, we observed how modified gravity impacted the SF. In the scenario of a GUP-corrected WH, we used the KMM model, as the behavior of the KMM and DGS models is similar. All the WH conditions were evaluated through 2D plots. Moreover, we plotted contour plots by varying the electric charge parameter and fixing the GB-coupled parameters. We also observed that $b(r)$ grows with growth in the value of the GB-coupled parameter in each case, but $b(r)$ is a declining function of electric charge. It was also found that $b'(r) < 1$ for $\mu < 0$, $\mu > 0$, $\mu = 0$. This condition is also satisfied for $Q > 0$, $Q < 0$ and $Q = 0$. The AF condition is not violated for $\mu > 0$ only. However, when μ is fixed, it is satisfied for $Q > 0$, $Q < 0$ and $Q = 0$.
- The NEC and WEC at the WH throat and far away from the throat were also explored. It was observed that the WEC in each case is violated due to the presence of negative Casimir energy density.
- We also studied $M_{\mathcal{A}}$ of a WH, which was developed in this article. The Casimir effect currently acts as a visible manifestation of such exotic matter. The presence of a negative $M_{\mathcal{A}}$ shows the existence of exotic matter. When measured in a particular area of space, the Casimir effect produces a negative value for $M_{\mathcal{A}}$. We studied the behavior of the $M_{\mathcal{A}}$ of a WH in each case for a constant value of Q, where we observed that $M_{\mathcal{A}}$ is negative for each case. In all cases, $M_{\mathcal{A}}$ decreases with increasing value of a, A and α. Further, we saw that when the electric charge increases, $M_{\mathcal{A}}$ increases. However, $M_{\mathcal{A}}$ decreases for the WH model developed from two concentric spheres with an increase in electric charge. For the GUP-corrected WH, $M_{\mathcal{A}}$ decays with increase in Q.
- Using mathematical models to characterize the developed WHs in both 3D and 2D spacetimes, we explored the geometry of WHs. The energy densities of these WHs are responsible for manifestation of charged Casimir phenomena. We noted that the SF $b(r)$ satisfies every prerequisite for the existence of a WH. In order to illustrate the geometry of the WH for various CCWH scenarios, specifically when t is held constant and θ is set to $\frac{\pi}{2}$, we presented graphical representations in the form of embedded diagrams. In addition, we presented two asymptotically flat WHs displaying a cosmos in both 3D and 2D spacetimes.
- We also studied the dynamics of the CF for each scenario in order to understand the system's complexity. Based on the values of μ and Q, we found that $\mathcal{Y}_{TF}$ constantly falls within a particular range, namely $-1 < \mathcal{Y}_{TF} \leqslant 0$. $\mathcal{Y}_{TF}$ tends to approach zero as we go away from the WH throat. The results in [43] show that a configuration with uniform energy density (ρ) and isotropic pressure has a null CF. In contrast, a CF can also be zero in the presence of an anisotropic pressure and an inhomogeneous energy density, provided that these two effects cancel each other out in the CF. In the present study, the CF exhibits a

Table 2. Main findings of WH conditions.

WH	Dynamics of $b(r)$	Asymptotic flatness condition	Flaring out condition
Case A	$b(r)>0\ \forall\ \mu$ except for $\mu=0$, $b(r)<0\ \forall\ Q$	$\forall\ \mu$ except $\mu=0$ and $\forall\ Q$	$\forall\ \mu$ except $\mu=0$ and $\forall\ Q$
Case B	$b(r)>0\ \forall\ \mu$ except for $\mu=0$, $b(r)<0\ \forall\ Q$	$\forall\ \mu$ except $\mu=0$ and $\forall\ Q$	$\forall\ \mu$ except $\mu=0$ and $\forall\ Q$
Case C	$b(r)>0\ \forall\ \mu$ except for $\mu=0$, $b(r)<0\ \forall\ Q$	$\forall\ \mu$ except $\mu=0$ and $\forall\ Q$	$\forall\ \mu$ except $\mu=0$ and $\forall\ Q$
Case D	$b(r)>0\ \forall\ \mu$ except for $\mu=0$, $b(r)<0\ \forall\ Q$	$\forall\ \mu$ except $\mu=0$ and $\forall\ Q$	$\forall\ \mu$ except $\mu=0$ and $\forall\ Q$

monotonic increase close to the WH throat while it slowly approaches zero for larger radial coordinates.

- Equilibrium forces for a CCWH for each case have been calculated and plotted. We found that for $r>6$ forces completely balance each other's effects.
- Casimir WHs in the background of EGB gravity were explored for the first time without considering the effects of electric charge in [70]; Casimir energy density was considered (energy density due to induction of the GUP effect and developed SF). The WH conditions were assessed in simple 2D plots and in terms of contour plots to find the dynamics of μ. Contour plots were plotted to understand the behavior of GB-coupled parameters in specific domains. Moreover, to measure the deviation of EGB gravity from GR, the findings in [70] were compared with the results found in [51]. The present manuscript is designed to explore the Casimir energy densities with the inclusion of electric charge by utilizing the idea presented in [60]. We considered different energy densities, developed the SF and evaluated their properties. By taking the influence of electric charge into consideration, we obtained an asymptotically flat SF. The behavior of the GB-coupled parameter μ and electric charge parameter Q were studied in detail. We observed that the presence of Q has a strong influence on the behavior of the SF. Moreover, by substituting $Q=0$ and $\epsilon_0=1$ in each result of the present article, we obtained the same outcomes as in [70]. Summary tables with all the findings are given below (tables 1 and 2).
- We also contrasted our findings with one from GR. We have two independent, maximally symmetric solutions for our acquired SF. Although it is possible for both solutions to exhibit different asymptotic behaviors GR does not exhibit this. The expression of the SF from GR is only dependent on radial distance r. In the case of EGB gravity, we have an additional parameter or degree of freedom to comprehend the dynamics. Similarly, EGB gravity has two degrees of freedom, μ and α, in the scenario of a CCWH with GUP correction.

The effects of Casimir energy densities within different modified theories have also been studied by many authors [52, 55, 56, 58], where they inculcated the ideas of Garattini, which he presented in [51]. In the current article, we used a newly introduced concept of Garattini, an extension of his previous work [60], and studied four different systems of Casimir energy density. Consequently, this research delivers a new perspective on the subject of CCWHs studied in higher-dimensional gravities.

Acknowledgments

Ali H Alkhaldi extends his appreciation to the Deanship of Research and Graduate Studies at King Khalid University for funding this work through a Large Research Project under Grant No. RGP2/453/45. The work of M Zubair has been partially supported by the National Natural Science Foundation of China under Grant No. 11988101. He is also grateful to the Compact Object and Diffused Medium Research Group at NAOC, led by Professor Jin Lin Han, for the excellent hospitality and friendly environment.

ORCID iDs

M Zubair https://orcid.org/0000-0003-2227-788X

References

[1] Einstein A and Rosen N 1935 The particle problem in the general theory of relativity *Phys. Rev.* **48** 73
[2] Morris M S and Thorne K S 1988 Wormholes in space-time and their use for interstellar travel: a tool for teaching general relativity *Am. J. Phys.* **56** 395
[3] Hochberg D and Visser M 1998 Null energy condition in dynamic wormholes *Phys. Rev. Lett.* **81** 746
[4] Hochberg D and Visser M 1998 Dynamic wormholes, antitrapped surfaces, and energy conditions *Phys. Rev.* D **58** 044021
[5] Cleement G, Galtsov D and Guenouche M 2016 NUT wormholes *Phys. Rev.* D **93** 024048
[6] Beato E A, Canfora F and Zanelli J 2016 Analytic self-gravitating Skyrmions, cosmological bounces and AdS wormholes *Phys. Lett.*B **752** 201
[7] Canfora F, Dimakis N and Paliathanasis A 2017 Topologically nontrivial configurations in the 4D Einstein-nonlinear σ-model system *Phys. Rev.* D **96** 025021
[8] Mehdizadeh M R and Ziaie A H 2017 Einstein–Cartan wormhole solutions *Phys. Rev.* D **95** 064049
[9] Parsaei F and Rastgoo S 2020 Wormhole solutions with a polynomial equation-of-state and minimal violation of the null energy condition *Eur. Phys. J.*C **80** 366
[10] Perlmutter S *et al* 1999 Measurements of omega and lambda from 42 high-redshift supernovae *Astrophys. J.* **517** 565
[11] Komatsu E *et al* 2011 Seven-year Wilkinson microwave anisotropy probe (WMAP*) observations: sky maps, systematic errors, and basic results *Astrophys. J. Suppl. Ser.* **192** 18
[12] Riess A G *et al* 2007 New Hubble Space Telescope discoveries of type Ia supernovae at $z\geqslant 1$: narrowing constraints on the early behavior of dark energy *Astrophys. J.* **659** 98
[13] Suzuki N *et al* 2012 The Hubble Space Telescope cluster supernova survey. V. Improving the dark-energy constraints

above $z > 1$ and building an early-type-hosted supernova sample *Astrophys. J.* **746** 85
[14] Buchdahl H A 1970 Non-linear Lagrangians and cosmological theory *Mon. Not. R. Astron. Soc.* **150** 1–8
[15] Starobinsky A 1980 A new type of isotropic cosmological models without singularity *Phys. Lett.*B **91** 99–102
[16] Harko T, Lobo F S N, Nojiri S and Odintsov S D 2011 $f(R, T)$ gravity *Phys. Rev.* D **84** 024020
[17] Lobo F S N and Oliveira M A 2009 Wormhole geometries in $f(R)$ modified theories of gravity *Phys. Rev.* D **80** 104012
[18] Visser M, Kar S and Dadhich N 2003 Traversable wormholes with arbitrarily small energy condition violations *Phys. Rev. Lett.* **90** 201102
[19] Jusufi K, Sarkar N, Rahaman F, Banerjee A and Hansraj S 2018 Deflection of light by black holes and massless wormholes in massive gravity *Eur. Phys. J.*C **78** 349
[20] Rahaman F, Paul N, Banerjee A, De S S, Ray S and Usmani A A 2016 The Finslerian wormhole models *Eur. Phys. J.*C **76** 246
[21] Sahoo P K, Moraes P H R S and Sahoo P 2018 Wormholes in R^2-gravity within the $f(R, T)$ formalism *Eur. Phys. J.*C **78** 46
[22] Tsukamoto N and Bambi C 2015 Strong deflection limit analysis and gravitational lensing of an Ellis wormhole *Phys. Rev.* D **91** 084013
[23] Ovgun A, Jusufi K and Sakalli I 2019 Exact traversable wormhole solution in bumblebee gravity *Phys. Rev.* D **99** 024042
[24] Shaikh R 2018 Shadows of rotating wormholes *Phys. Rev.* D **98** 024044
[25] Tsukamoto N, Harada T and Yajima K 2012 Can we distinguish between black holes and wormholes by their Einstein ring systems *Phys. Rev.* D **86** 104062
[26] Jusufi K, Banerjee A, Gyulchev G and Amir M 2019 Distinguishing rotating naked singularities from Kerr-like wormholes by their deflection angles of massive particles *Eur. Phys. J.C* **79** 28
[27] Kord Zangeneh M, Lobo F S N and Riazi N 2014 Higher-dimensional evolving wormholes satisfying the null energy condition *Phys. Rev.* D **90** 024072
[28] Lobo F S N 2007 General class of braneworld wormholes *Phys. Rev.* D **75** 064027
[29] Lobo F S N and Oliveira M A 2009 Wormhole geometries in $f(R)$ modified theories of gravity *Phys. Rev.* D **80** 104012
[30] Garcia N M and Lobo F S N 2010 Wormhole geometries supported by a nonminimal curvature-matter coupling *Phys. Rev.* D **82** 104018
[31] Boehmer C G, Harko T and Lobo F S N 2012 Wormhole geometries in modified teleparallel gravity and the energy conditions *Phys. Rev.* D **85** 044033
[32] Capozziello S, Harko T, Koivisto T S, Lobo F S N and Olmo G J 2012 Wormholes supported by hybrid metric-Palatini gravity *Phys. Rev.* D **86** 127504
[33] Dehghani M H and Dayyani Z 2009 Lorentzian wormholes in Lovelock gravity *Phys. Rev.* D **79** 064010
[34] Lovelock D 1971 The Einstein tensor and its generalizations *J. Math. Phys.* **12** 498
[35] Bhawal B and Kar S 1992 Lorentzian wormholes in Einstein–Gauss–Bonnet theory *Phys. Rev.* D **46** 2464
[36] Mehdizadeh M R and Riazi N 2012 Dynamical wormholes in Lovelock gravity *Phys. Rev.* D **85** 124022
[37] Rahaman F, Kuhfittig P K F, Ray S and Islam S 2012 Searching for higher-dimensional wormholes with noncommutative geometry *Phys. Rev.* D **86** 106010
[38] Torii T and Shinkai H-a 2013 Wormholes in higher dimensional space-time: exact solutions and their linear stability analysis *Phys. Rev.* D **88** 064027
[39] Sokoliuk O and Baransky A 2021 On the existence and stability of traversable wormhole solutions in modified theories of gravity *Eur. Phys. J.*C **81** 781
[40] Antoniou G, Bakopoulos A, Kanti P, Kleihaus B and Kunz J 2020 Novel Einstein–scalar-Gauss–Bonnet wormholes without exotic matter *Phys. Rev.* D **101** 024033
[41] Godani N, Singh D V and Samanta G C 2022 Stability of thin-shell wormhole in 4D Einstein–Gauss–Bonnet gravity *Phys. Dark Univ.* **35** 100952
[42] Zubair M, Farooq M, Gudekli E, Kousar H R and Yildiz G D A 2023 No AccessNew traversable wormhole solutions in Einstein–Gauss–Bonnet gravity *Int. J. Geom. Methods Mod. Phys.* **20** 2350191
[43] Herrera L 2018 New definition of complexity for self-gravitating fluid distributions: the spherically symmetric, static case *Phys. Rev.* D **97** 044010
[44] Herrera L, Di Prisco A, Fuenmayor E and Traconis O 2009 Dynamics of viscous dissipative gravitational collapse *Int. J. Mod. Phys.*D **18** 129
[45] Herrera L, Barreto W, Di Prisco A and Santos N O 2002 Relativistic gravitational collapse in noncomoving coordinates: the post-quasistatic approximation *Phys. Rev.* D **65** 104004
[46] Herrera L and Santos N O 2004 Dynamics of dissipative gravitational collapse *Phys. Rev.* D **70** 084004
[47] Herrera L, Di Prisco A, Martin J, Ospino J, Santos N O and Troconis O 2004 Spherically symmetric dissipative anisotropic fluids: a general study *Phys. Rev.* D **69** 084026
[48] Sharif M, Majid A and Nasir M M M 2019 Complexity factor for self-gravitating system in modified Gauss–Bonnet gravity *Int. J. Mod. Phys.*D **34** 1950210
[49] Abbas G and Ahmed R 2019 Complexity factor for a class of compact stars in $f(R, T)$ gravity *Astrophys. Space Sci.* **364** 194
[50] Abbas G and Nazar H 2018 Complexity factor for anisotropic source in non-minimal coupling metric f(R) gravity *Eur. Phys. J.*C **78** 957
[51] Garattini R 2019 Casimir wormholes *Eur. Phys. J.*C **79** 951
[52] Jusufi K, Channuie P and Jamil M 2020 Traversable wormholes supported by GUP corrected Casimir energy *Eur. Phys. J.*C **80** 127
[53] Jusufi K, Moulay E, Mureika J and Farag Ali A 2023 Einstein–Rosen bridge from the minimal length *Eur. Phys. J.*C **83** 282
[54] Javed W, Hamza A and Ovgun A 2020 Weak deflection angle by Casimir wormhole using Gauss–Bonnet theorem and its shadow *Mod. Phys. Lett.*A **35** 2050322
[55] Tripathy S K 2021 GUP corrected Casimir wormholes in $f(Q)$ gravity *Phys. Dark Univ.* **31** 100757
[56] Sokoliuk O, Baransky A and Sahoo P K 2022 Probing the existence of the ZTF Casimir wormholes in the framework of $f(R)$ gravity *Nucl. Phys.*B **980** 115845
[57] Muniz C R, Bezerra V B and Toledo J M 2021 Casimir effect in space-times of rotating wormholes *Eur. Phys. J.*C **81** 209
[58] Hassan Z, Ghosh S, Sahoo P K and Bamba K 2022 Wormhole solutions in $f(Q, T)$ gravity with a radial dependent B parameter *Eur. Phys. J.*C **82** 1116
[59] Avalos R, Fuenmayor E and Contreras E 2022 Traversable wormholes with like Casimir complexity supported with arbitrarily small amount of exotic matter *Eur. Phys. J.*C **82** 420
[60] Garattini R 2023 Effects of an electric charge on Casimir wormholes: changing the throat size *Eur. Phys. J.*C **83** 369
[61] Casimir H 1948 On the attraction between two perfectly conducting plates *Proc. K. Ned. Akad. Wet.* **51** 793
[62] Sparnaay M 1957 Attractive forces between flat plates *Nature* **180** 334
[63] Samart D, Tangphati T and Channuie P 2022 Charged traversable wormholes supported by Casimir energy with and without GUP corrections *Nucl. Phys.*B **980** 115848
[64] Lombardo F C, Mazzitelli F D and Villar P I 2008 Exploring the quantum vacuum with cylinders *J. Phys. A, Math. Theor.* **41** 164009

[65] Straley J P and Kolomeisky E B 2017 Casimir interaction of arbitrarily *J. Phys. Condens. Matter* **29** 143002
[66] Kempf A, Mangano G and Mann R B 1995 Hilbert space representation of the minimal length uncertainty relation *Phys. Rev.* D **52** 1108
[67] Detournay S, Gabriel C and Spindel P 2002 About maximally localized states in quantum mechanics *Phys. Rev.* D **66** 125004
[68] Frassino A M and Panella O 2012 Casimir effect in minimal length theories based on a generalized uncertainty principle *Phys. Rev.* D **85** 045030
[69] Kempf A and Mangano G 1997 Minimal length uncertainty relation and ultraviolet regularization *Phys. Rev.* D **55** 7909
[70] Zubair M and Farooq M 2023 Imprints of Casimir wormhole in Einstein–Gauss–Bonnet gravity with non-vanishing complexity factor *Eur. Phys. J.*C **83** 507